Distinct Non-occluding Functions of Septate Junction Components in Signaling Pathway Regulation and Cell Polarity During Epithelial Development

Holtwick, V., Schubert, A. and Rust, K.*

Institute of Physiology and Pathophysiology, Dept. of Molecular Cell Physiology, Philipps University Marburg, Germany

*to whom correspondence should be addressed:
rustka@staff.uni-marburg.de

Key words:

Septate junction, occluding junction, follicle epithelium, cell polarity, actin cytoskeleton, Wnt signaling, Jak-STAT signaling.

Abstract

Occluding junctions are essential for tissue integrity and barrier function in epithelial tissues. Here we identify several non-occluding functions of septate junction components, the invertebrate occluding junctions, in follicle epithelium development. We show that the morphogenesis of the follicular stalk is an actin-driven process that requires intact apical-basal cell polarity, which is controlled by septate junction components. Septate junction components further regulate signaling pathways in a cell-type specific manner. In undifferentiated stem cells and immediate daughters, septate junction components promote effective Wnt signaling to control proliferation, while they limit Jak-STAT signaling activity induced by polar cells. Together, our data emphasize the multiple roles of septate junction components independent of their classical role in forming the paracellular barrier.

Introduction

Functional epithelial tissues are vital for organismal development and health. Epithelial homeostasis and development require a tight coordination of proliferation, differentiation and cell morphological changes. The *Drosophila* follicle cell lineage depicts an excellent model to study epithelial development from a highly proliferative niche-maintained stem cell to a single layered mature epithelium. Follicle cells are produced in the germarium by follicle stem cells, which obtain

niche signals from neighboring escort cells and cap cells [1–4]. Follicle stem cells divide to produce transiently amplifying prefollicle cells which associate with developing germline cysts and differentiate. The first differentiation choice prefollicle cells can undergo is induced by Delta, which is produced by germline cysts in Region 2b [5–7]. Delta receiving prefollicle cells differentiate into polar cells, which form two clusters of signal producing cells on either side of the germline cyst. Polar cells then produce the Jak-STAT ligand Unpaired (Upd) and pattern the surrounding follicle epithelium. Neighboring follicle cells that receive Upd in the germarium differentiate into stalk cells and form a single row of cells connecting two neighboring germline cysts [6,8,9]. The remaining prefollicle cells differentiate into main body follicle cells, which organize into a single layer epithelium that ensheaths the germline cyst. (Fig. 1a).

The follicle epithelium possesses classical epithelial properties, including apical-basal polarity and cellular junctions [10,11]. Among epithelial junctions, septate junctions are invertebrate cell-cell junctions that localize to the lateral membrane and assume a barrier function similar to vertebrate tight junctions [12]. Based on their appearance in ultrastructural microscopy and molecular composition, mature septate junctions are classified in either pleated, ladder-like septate junctions (pSJ) or smooth septate junctions (sSJ). Further, septate junctions can form as tricellular junctions (tSJ). Septate junctions are formed by roughly thirty different components [13]. Among the core components are the Claudin homolog Kune-kune (kune), the transmembrane protein Nrx-IV, which in turn interacts with the FERM domain of the cytoskeleton-interacting protein Coracle (Cora), as well as the α and β subunits of the Na^+/K^+ ATPase ATPα and Nrv2, which both assume ion-pump-independent roles in septate junction formation [13–20]. Molecularly, septate junctions are conserved to vertebrate septate junctions, known as axo-glial septate junctions, in myelinated axons [21]. In the follicle epithelium, septate junction components are universally expressed [22]. Yet, septate junctions only assemble into incipient septate junctions at Stage 6 and are visible as mature, pleated septate junctions from Stage 10 onwards [11], suggesting that septate junction components assume non-occluding functions during follicle epithelium development. While the molecular mechanisms are not fully described, septate junction components fulfill non-occluding functions in other systems, where they regulate processes like cell migration, cell-cell communication, cell adhesion and polarity as well as proliferation [13,23]. In the late follicle epithelium, septate junction proteins are required for egg elongation and the formation of dorsal appendages, which are formed from late stage main body follicle cells [24]. They are also required for border cell migration, where the anterior polar cells and surrounding outer border cells

delaminate and migrate through the nurse cells towards the oocyte [24,25]. However, the mechanism behind septate junction component function in follicle epithelium morphogenesis is unclear.

Here we study the septate junction core components Cora, Kune, Nrv2 and Nrx-IV in the early follicle cell lineage of *Drosophila melanogaster*. We identify several cell type specific and non-occluding roles of septate junction components, which are crucial for normal follicle cell development. We show, for the first time, that septate junction components regulate Wnt signaling activity in follicle stem cells and prefollicle cells, thereby regulating their proliferation and ensuring normal encapsulation of germline cysts. Further, we characterize the morphogenesis of the follicular stalk and show that this process is dependent on E-Cadherin, apical-basal polarity and the actin cytoskeleton, all of which are coordinated by septate junction components. Lastly, septate junction components are required in polar cells, where they regulate cell polarity to limit the availability of the Jak-STAT ligand Upd, which controls stalk cell numbers.

Results

Normal follicle epithelium formation relies on septate junction genes

Septate junction components are highly expressed in differentiated main body follicle cells [22] but their expression during early follicle epithelium formation is poorly described. Using a single cell RNA-sequencing dataset of the *Drosophila* ovary [7], we investigated the expression of genes encoding septate junction components in somatic cells of early stages of oogenesis. Several septate junction genes including *cora* and *nrv2* display high expression in escort cells (Fig. 1b). Polar cells exhibit enriched expression for many septate junction genes including *Gli*, *bark* and *M6*, which encode components contributing to tricellular septate junctions. *Nrg* is further highly expressed in stalk cells, while other follicle cell types express lower levels of septate junction genes. Indeed, Nrx-IV-mCherry is expressed in all somatic cells of the ovary with higher levels in escort cells and strongest expression in polar cells, as predicted (Fig. 1b-c). Further, using antibody staining we detected Cora expression in escort cells as well as all types of follicle cells (Fig. 1d). In follicle cells Cora localized to the lateral membrane and we detected the highest Cora staining in mature stalk cells (Fig. 1d).

To investigate the function of septate junctions in the follicle epithelium we examined knockdown of the core septate junction components *cora*, *nrv2*, *Nrx-IV* and *kune*. To this aim, we employed the pan-follicle cell Gal4 driver 109-30-Gal4 [26] combined with tub-Gal80^{ts} (hereafter referred to as

^{ts}) to target the adult follicle epithelium (Fig. S1a). To validate the knockdown of *cora* we stained the ovaries with *cora* knockdown in follicle cells with an anti-Cora antibody. When compared to control, Cora staining was strongly reduced in follicle cells while escort cells, which are not targeted by 109-30^{ts}, displayed unaltered Cora expression (Fig. S1b-c). Septate junction components including Cora localize laterally [27]. Consistently, Cora staining was highest in the lateral domain of wildtype main body cell membranes in Stage 6 (Fig. 1e). In contrast, knockdown of *kune*, *nrv2* or *Nrx-IV* shifted Cora localization towards the apical portion of the lateral cell membrane (Fig. 1f-i), in agreement with the interdependent localization of septate junction components.

Having confirmed the functionality of RNAi lines, we next examined the morphological phenotypes of ovaries upon 109-30^{ts}-induced knockdown of *cora*, *kune*, *nrv2* or *Nrx-IV*. Interestingly, we found that depletion of *cora*, *kune*, *nrv2* or *Nrx-IV* resulted in similar morphological defects. While wildtype germaria contained on average 1.76 ± 0.1 follicle cell encapsulated cysts in Region 2b, knockdown of these septate junction proteins significantly increased the number of follicle cell encapsulated cysts in this region (Fig. 1j-m, S1d-e, *cora* #35003: 2.86 ± 0.19, *cora* #51845: 2.86 ± 0.19, *kune* #38925: 2.67 ± 0.16, *nrv2* #28666: 3.07 ± 0.14, *nrv2* #37495: 2.93 ± 0.25, *Nrx-IV* #32424: 3.06 ± 0.11 cysts per Region 2b). Only 6.47 % of control germaria contained more than two cysts in Regions 2b, while knockdown of septate junction components significantly increased the percentage of ovaries with more than two cysts (Fig. S1f). Knockdown of septate junction genes further resulted in a lack of cyst stages. While the second budded cyst in wildtype ovaries was either in Stage 3 or 4 (56% and 44%, respectively), the second budded cysts in ovaries with septate junction gene knockdown were significantly older regarding their developmental stage (Fig. S1g). Lastly, when we stained ovarioles for Hu li tai shao (Hts), which is expressed in the entire follicle epithelium, we noted that stalks were double rowed in comparison to the single row morphology observed in wildtype (Fig. 1n-p, S1h-j). While wildtype stalks contained on average 6.86 ± 0.15 cells per stalk, knockdown of septate junction components *cora*, *kune*, *nrv2* or *Nrx-IV* significantly increased stalk cell numbers (Fig. 1q). The morphological defects caused by depletion of *cora*, *nrv2*, *Nrx-IV* or *kune* indicate that these septate junction proteins are vital for follicle cell morphogenesis and encouraged us to further explore their function in follicle epithelial development.

Septate junction components regulate FSC and pFC proliferation via Wnt signaling

Loss of septate junctions affects proliferation in other types of epithelia [28–30]. Thus, the expansion of the stalk cell number upon septate junction gene knockdown prompted us to investigate proliferation. We quantified the percentage of EdU labeled cells upon pan-follicle knockdown of septate junction genes and found that, as in the wildtype, stalk cells are quiescent outside of the germarium (Fig. S2a-e, no EdU positive stalk cells from 109-30^{ts} crossed to *w^{1118}*, *cora* #35003, *cora* #51845, *kune* #38925, *nrv2* #28666, *nrv2* #37495, *Nrx-IV* #32424, n = 9, 11, 10, 14, 10, 11, 8 ovarioles respectively). The expansion of the stalk cell pool is therefore not caused by a failure of differentiated stalk cells to exit mitosis. To investigate whether the increased stalk cell numbers might be caused by an elevated proliferation rate of FSCs or pFCs we quantified EdU positive somatic cells in Region 2b of the germarium. We found that knockdown of septate junction genes with the pan-follicle cell driver 109-30^{ts} significantly reduced the percentage of EdU positive follicle cells in Region 2b (Fig. 2a, *w^{1118}*: 22.9 ± 3.27%, *cora* #35003: 6.55 ± 0.93%, *cora* #51845: 11.26 ± 2.81%, *kune* #38925: 8.73 ± 1.91%, *nrv2* #28666: 12.18 ± 2.64%, *nrv2* #37495: 7.71 ± 1.99%, *Nrx-IV* #32424: 9.42 ± 3.05%). To test whether septate junction component knockdown generally reduced proliferation of dividing cells, we assessed EdU incorporation of main body follicle cells shortly before they exit mitosis in Stage 6. However, EdU incorporation in main body follicle cells was not affected (Fig. 2b).

Various signaling pathways regulate FSC and pFC proliferation, including the Wnt signaling pathway [2,8]. We tested the influence of *cora* and *nrv2* knockdown on the Wnt pathway reporter fz3::RFP and found a significant reduction of Wnt signaling activity in Region 2b follicle cells (Fig. 2c-f). This reduction of Wnt signaling is likely responsible for the reduced proliferation of FSCs and pFCs (Fig. 2a). We postulated that the reduced proliferation in Region 2b is responsible for the cyst encapsulation defects (Fig. 1j-m, S1d-e). Indeed, reduction of Wnt signaling by RNAi-knockdown of the genes encoding the Wnt signaling effector β-Catenin (*arm*) or the positive regulator of Wnt signaling *dishevelled* (*dsh*) resulted in an increase of germline cysts in Region 2b, similar to the knockdown of septate junction core components (Fig. 2g-j, *w^{1118}*: 1.88 ± 0.08, *arm*: 3.38 ± 0.21, *dsh*: 2.56 ± 0.23 cysts per germarium). Together, septate junction components regulate FSC and pFC proliferation via Wnt signaling, which is required for effective production of follicle cells to encapsulate germ cell cysts entering the follicle cell region. Further, the double row stalk cell phenotype observed upon septate junction gene depletion is not caused by excessive proliferation of FSCs or pFCs.

Differentiation and apoptosis are not affected by septate junction components

In order to examine whether the double row stalk phenotype is caused by faulty differentiation, we examined cell type specific markers for the early stages of follicle cell development. In wildtype, Aop is expressed in all stalk cells, while LamC displays low expression in the first stalk and high expression in later stalk cells [7,31,32]. Zfh1 is expressed in FSCs and pFCs and retains strong expression in stalk cells but is downregulated in main body follicle cells and polar cells [7]. Eya is expressed in FSCs and pFCs and while main body follicle cells maintain Eya expression, stalk and polar cells downregulate Eya [33]. Examination of ovaries with knockdown of septate junction genes revealed that neither of these cell fate markers were misexpressed, suggesting that stalk cells differentiate normally (Fig. 2k-v, S2f-m). A previous study claimed that stalk cell numbers are fine-tuned via stalk cell apoptosis [34]. To test whether septate junction component knockdown affects the rate of apoptosis we stained ovaries with pan-follicle cell knockdown of septate junction genes for the apoptotic marker cleaved death caspase 1 (c-Dcp-1). While our staining identified polar cells, marked by high Fas3 expression, undergoing apoptosis as expected, we did not observe c-Dcp-1 positive stalk cells marked by LamC in either wildtype ovaries or ovaries with septate junction gene knockdown (Fig. S2n). Septate junction genes therefore do not regulate stalk cell numbers via apoptosis. While we did not note any defects in either differentiation or apoptosis, we noted that stalk cells with septate junction component knockdown maintained high Fas3 expression in stalks, while wild type stalk cells decreased Fas3 expression from Stage 3 onwards [7,35] (Fig. S2o). This suggests that septate junction knockdown affects cell membrane organization in stalk cells.

Septate junction components regulate actin and cell polarity to promote stalk morphogenesis

Cell membrane organization is regulated by the apical-basal polarity machinery in epithelial cells. In fact, septate junctions are required for normal apical-basal polarity as well as cytoskeleton organization in the embryonic epithelium [36,37]. Since the importance of cell polarity and cytoskeleton dynamics is unclear during stalk development, we first sought to characterize stalk morphogenesis in more detail. Stalk formation has previously been classified into distinct steps starting: Initiation in Region 2b, where stalk cells are specified; Convergence in Region 3, where stalk cells start contacting each other; Intercalation into a single row stalk in Stage 3; and Closing in Stages 4-5 where the extracellular matrix is reorganized [38]. We stained wildtype stalk for E-Cad, as a marker for adherens junctions, and Phalloidin to visualize the F-actin cytoskeleton (Fig.

3a-f). During initiation E-Cad and F-actin start to accumulate between stalk cell precursors located between the two lens shaped germline cyst in Regions 2b and 3 (Fig. 3a, g). When germline cysts are advanced in Region 3, characterized by rounded cysts, E-Cad and F-actin are accumulated between stalk cells, which have started constricting (Fig. 3b, g). As cysts advance further they bud off the germarium, which is characterized by a morphologically recognizable stalk region. Here stalk cells have formed a double row and display a consistent line of E-Cad and high F-actin between them, which forms a “zipper” line across the intercalating stalk cells (Fig. 3c, g). Intercalation does not occur between all stalk cells simultaneously. Instead, the first stalk usually displays mostly a single row of stalk cells while few stalk cells are still in the process of intercalation (Fig. 3d, g). The second stalk is often fully intercalated, although we noticed some variation, and here stalk cells display spots of E-Cad between them (Fig. 3e, g). The third stalk is normally matured and displays E-Cad localization laterally between stalk cells (Fig. 3f-g). Through these stages of stalk development we found that Cora was lowly expressed in early stages of stalk formation with erratic localization and moves laterally as the stalk matures (Fig. S3a-f). To better understand the intercalation process, we applied live imaging using endogenously tagged E-Cad. We found that the process from budding, where a “zipper” line of E-cad is visible between a double row of stalk cells, to intercalation, where E-Cad is mostly visible as spot-like accumulations between stalk cells, occurs in a matter of a few hours (Fig. 3h-j).

As the double row phenotype evoked by knockdown of *cora*, *nrv2*, *Nrx-IV* and *kune* indicates defects in stalk cell intercalation, we focused on the budding stage, where stalk cells are present in a double row in the wildtype (Fig. 1i-k, S1g-h, 3c). Using three-dimensional image analysis, we confirmed that E-Cad localizes in a single, consistent line between stalk cells in the wildtype (Fig. 4a, note the cross-sections). In contrast, pan-follicle cell knockdown of *cora*, *nrv2*, *Nrx-IV* and *kune* resulted in a range of defects including the formation of multiple E-Cad lines, indicating incomplete contact between stalk cells, inconsistent and broken E-Cad lines and mislocalization to the outer, basal side of stalk cells (Fig. 4b-c, S3g-h, note the cross-sections).

Next, we assessed markers of apical-basal polarity. Bazooka (Baz), an apical polarity marker, localizes to the E-Cad zipper line in budding stalks in wildtype (Fig. 4d). Knockdown of septate junction components resulted in inconsistent zipper lines for E-Cad as well as Baz (Fig. 4e-f, S3i-j). Additionally, E-Cad and Baz expression were reduced as indicated by a reduced fluorescence intensity upon knockdown of *cora*, *nrv2*, *Nrx-IV* or *kune* (Fig. 4g-h). Discs large 1 (Dlg), a basolateral polarity protein, was absent from the zipper line in wildtype and instead localized to

the lateral membranes of budding stalk cells (Fig. 4i). In contrast, upon septate junction component knockdown, Dlg frequently co-localized with F-actin at the zipper line (Fig. 4j-l, S3k-l). Lastly, wildtype budding stalk cells displayed high levels of F-actin at the apical zipper line and lower F-actin levels at the basal side, while budding stalk cells with knockdown of *cora*, *nrv2*, *Nrx-IV* or *kune* did not establish this gradient (Fig. 4m). To test whether these defects are indeed responsible for the double row stalk phenotype, we depleted *E-Cad* (encoded by *shotgun*) from follicle cells by RNAi-knockdown. Indeed, knockdown of *E-Cad* resulted in cyst fusions and double row stalks, indicating defects in stalk cell intercalation (Fig. S3m). In summary, septate junction components regulate cell polarity, adhesion and F-actin localization to promote stalk cell intercalation.

Septate junction components control stalk cell number via Jak-STAT signaling

While the defective actin cytoskeleton and cell polarity causes stalk cell intercalation resulting in double rowed stalks observed in septate junction knockdown, it is unlikely that these defects cause the increased stalk cell number (Fig. 1l). Accordingly, stalk cell specific knockdown of septate junction components with the stalk cell specific driver CG46339^{ts} [7] resulted in double rowed stalks but did not increase stalk cell numbers (Fig. 5a-d, S4a-h).

Having established that the stalk cell defects observed upon septate junction component knockdown is not caused by overproliferation (Fig. 2a. S2a-e), we postulated that an increased number of stalk cells is specified from the prefollicle cell pool. Stalk cell specification is regulated by polar cells in the germarium, which produce Unpaired (Upd) to induce Jak-STAT signaling in neighboring prefollicle cells and direct them to differentiate towards the stalk cell fate [9]. First, we examined polar cell numbers, hypothesizing that an increased number of polar cells would induce more cells to specify as stalk cells. We found that similar to wildtype ovaries, ovaries with knockdown of septate junction components contained on average two polar cells (wildtype: 1.87 ± 0.06 polar cells, cora #35003: 1.83 ± 0.11, cora #51845: 1.91 ± 0.09, kune #38925: 2 ± 0, nrv2 #28666: 1.96 ± 0.07, nrv2 #37495: 1.92 ± 0.1, Nrx-IV #32424: 1.93 ± 0.08 cells per anterior polar cell cluster in Stage 3-4, p = ns, n = 31, 12, 11, 7, 25, 24, 30 respectively). Next, to test whether faulty Upd distribution from polar cells causes elevated stalk cell numbers, we targeted septate junction genes for knockdown with the polar cell driver upd^{ts} [33]. Indeed, polar cell specific knockdown resulted in a significant expansion of stalk cell numbers and was associated with a double row phenotype (Fig. 5e-h, S4i-n). Astonishingly, septate junction components thus function non-cell autonomously to regulate stalk cell numbers via polar cells. Consistently, we examined

the Jak-STAT reporter 2xSTAT-GFP and found that knockdown of septate junction components significantly increased Jak-STAT signaling levels in stalk cells and main body follicle cells, in which Jak-STAT signaling is induced by polar cells. In contrast, Jak-STAT signaling was not elevated in the FSC/pFC Region 2b, where Jak-STAT signaling is induced independently of polar cells (Fig. 5i-l, S4o). Hence, the increased stalk cell number upon septate junction gene knockdown is caused by elevated Jak-STAT signaling induced by polar cells.

A previous study showed that *upd1*-mRNA is apically localized in polar cells [39]. Stalk cells face the basal side of polar cells, hence disturbed polar cell polarity may increase the availability of Upd1 ligand for stalk cells. We tested whether Upd1 protein is apically enriched in polar cells and indeed HA-tagged Upd1 primarily localized to the apical side of polar cells across all stages (Fig. 6a). To test whether septate junction components regulate apical-basal polarity of polar cells, we investigated the localization of the adherens junction protein E-Cad, which localizes apically in epithelial cells, and F-actin, which is usually enriched at adherens junctions. We further stained for Fas3, which is highly expressed in polar cells. Interestingly, we found that Fas3, E-Cad and F-actin are enriched at the apical domain of polar cells in wildtype ovaries (Fig. 6a-d, S5a-b). Such a pronounced apical domain, referred to as the apical cap domain, has previously been reported for anterior polar cells during the process of border cell migration [40,41]. Remarkably, knockdown of *cora*, *nrv2*, *Nrx-IV* or *kune* particularly decreased localization of Fas3 to the apical cap and reduced F-actin enrichment but did not have a large effect on E-Cad apical localization (Fig 6b,d, S5b-c). In conclusion, septate junction components regulate polar cell polarity which plausibly affects Upd1 availability for surrounding follicle cells, thereby limiting the number of specified stalk cells.

Discussion

In this study we identified several functions for Cora, Nrv2, Nrx-IV and Kune during follicle epithelial development unrelated to the occluding function of septate junctions (Fig. 6e). These septate junction proteins facilitate Wnt signaling in undifferentiated follicle cells to ensure normal proliferation levels, which is the prerequisite for effective germline cyst encapsulation. They further regulate polar cell polarity thereby fine-tuning Jak-STAT signaling levels in surrounding follicle cells. Lastly, septate junction proteins are vital for normal stalk morphogenesis by maintaining apical-basal polarity and governing F-actin enrichment on the apical side, which provide driving forces for the stalk cell intercalation process. Together, our study demonstrates that septate

junctions are indispensable for normal epithelial development in the *Drosophila* ovary and assume distinct and cell type specific functions far beyond their role as occluding junctions.

Septate junction proteins regulate proliferation via the Wnt signaling pathway

Septate junction proteins have been linked to proliferation in the midgut epithelium, where they limit intestinal stem cell proliferation, and in the imaginal disc epithelium, where *cora* promotes proliferation [28–30]. We found that septate junction components are required for sustained FSC and pFC proliferation but are dispensable for main body follicle cell proliferation. This highlights that regulation of proliferation by septate junction components is highly tissue specific. We identify a previously unrecognized function of septate junction components in promoting Wnt signaling to induce proliferation. Depletion of septate junction genes or positive regulators of Wnt signaling similarly results in an accumulation of cysts in Region 2b, where germline cysts are first encapsulated by follicle cells. Normal levels of proliferation, regulated by septate junction proteins through Wnt signaling activity, thus are necessary to ensure the production of sufficient prefollicle cells to populate entering germline cysts.

How septate junction components regulate Wnt signaling is unclear. Frizzled proteins, the receptors for the Wnt family of signaling ligands, display apical-basal polarization in *Drosophila* as well as mammals [42,43]. Therefore, septate junctions may be required for normal polarity of FSCs and pFCs and thus Wnt pathway efficiency. However, in FSCs and pFCs classical apical-basal polarity is not yet established [44] and we also did not observe polarized Fz3 localization in Region 2b cells. Alternatively, septate junctions may be required for FSC adhesion thereby regulating exposure to Wnt ligands provided by niche cells. One apparent candidate is E-Cad, which is crucial for FSC niche adhesion [45] and is regulated by septate junction proteins in stalk cells. However, we did not observe any obvious changes in E-Cad localization or expression in Region 2b follicle cells upon septate junction component knockdown (data not shown). A previous study has suggested a role for the septate junction protein Neuroglian in lateral cell adhesion and septate junction proteins likely regulate cell-cell adhesion during border cell migration in Stages 9 to 10 egg chambers [22,46]. These findings point to the exciting possibility that septate junction proteins may be directly required for FSC niche adhesion.

Septate junction proteins regulate Jak-STAT signaling in the follicle epithelium

During follicle epithelium formation, septate junction proteins regulate not only Wnt but also Jak-STAT signaling. By controlling the normal composition of the apical cap region in polar cells, septate junction proteins evidently contribute to apical localization of Upd1 and thereby limit Jak-STAT signaling in ligand receiving cells to define the number of specified stalk cells. Septate junction proteins also regulate egg chamber elongation during late stages of oogenesis although the underlying mechanism is not understood [22]. Importantly, egg chamber elongation is dependent on Jak-STAT signaling induced by polar cells and overexpression of Upd results in failed elongation [47]. Our data suggest that septate junction proteins regulate egg chamber elongation via the maintenance of normal cell polarity in polar cells, which allows the establishment of the appropriate Upd gradient and Jak-STAT pathway activity in main body follicle cells.

Interestingly, in the midgut epithelium smooth septate junction members directly interact with the Hippo signaling effector Yorkie to limit Upd ligand expression [28,29]. In polar cells, forced nuclear entry of Yorkie results in the loss of polar cells and subsequently stalk cells [48]. Since septate junction component depletion does not alter polar cell numbers, they arguably do not regulate Jak-STAT activity via Hippo signaling in the follicle epithelium. Instead, they regulate aspects of cell polarity in polar cells, which can contribute to the apical localization and thereby distribution of Upd1. Fascinatingly, our study and others therefore show that septate junction components regulate the Jak-STAT signaling pathway in distinct, cell-type specific ways [28,29].

Cell polarity and the actin cytoskeleton are required for stalk cell intercalation

Septate junction components regulate stalk cells in a non-cell autonomous way via polar cells but are further cell autonomously required for proper stalk development. Stalk cell morphogenesis is a poorly understood process. While it is known that the basement membrane is important for stalk cell morphogenesis, cell polarity and cytoskeleton dynamics have not been investigated [38]. Here, we describe the distinct steps of stalk cell morphogenesis and provide evidence that E-Cad-mediated cell adhesion and the actin cytoskeleton are key drivers of stalk intercalation. Using *ex vivo* live imaging, we further show that stalk cell intercalation occurs over the course of a few hours. Septate junction proteins are required for normal localization of E-Cad and of the polarity proteins Baz and Dlg. Moreover, septate junction proteins are vital for apical accumulation of F-actin in intercalating stalk cells. Septate junctions have also been shown to regulate E-Cad and

actomyosin during dorsal closure in *Drosophila* embryonic development and mediate actin dynamics during wound closure [37,49]. Together, these data support a central role of septate junction proteins in dynamic processes dependent on cellular reorganization.

Conserved non-barrier functions of occluding junctions

Septate junction proteins, including Cora, Nrv2, Nrx-IV and Kune, are conserved in vertebrates, where their homologs contribute to axo-glial septate junctions [21,50]. These vertebrate septate junctions, similar to their invertebrate counterpart, form a diffusion barrier for paracellular transport and limit lipid exchange along the cell membrane. Consistently, mutations in axo-glial septate junction genes are associated with a range of different neuropathies [50]. While non-occluding functions of axo-glial septate junctions have not yet been described, tight junctions, vertebrate epithelial occluding junctions, fulfill several non-barrier functions. Like septate junctions, they reciprocally interact with the apical-basal polarity machinery [51]. Data from our study and others show that this function is conserved in invertebrate occluding junctions (this study and [36]). Tight junctions have also been linked to cell cycle regulation but a recent review highlights that the interplay with proliferation regulating signaling pathways is insufficiently understood [52]. In this study we identify a novel link between septate junction components and the Wnt and Jak-STAT signaling pathways. Other research has established that septate junction components further regulate Hippo signaling [53,54]. It is plausible that vertebrate occluding junctions similarly regulate a variety of signaling pathways that coordinate proliferation and differentiation. This association is of particular interest in the background of a growing body of evidence that connects tight junctions to cancer development [52].

Material and Methods

Fly husbandry and fly stocks

Flies were reared under standard lab conditions. All crosses including a tub-Gal80^{ts} construct were reared at 18°C and hatched offspring were transferred to 29°C for 14 days and fed wet yeast daily until dissection.

The following stocks were used in this study:

BDSC: *w^{1118}* (3605), 109-30-Gal4 (7023), CG46339-Gal4 (77710), tub-Gal80ts (7108), UAS-*cora*-RNAi (35003), UAS-*cora*-RNAi (51845), UAS-*kune*-RNAi (38295), UAS-*nrv2*-RNAi (28666), UAS-*nrv2*-RNAi (37495), UAS-*Nrx-IV*-RNAi (32424), UAS-*shg*-RNAi (32904), UAS-2XStat92E-GFP

(26196), Nrx-IV-mCherry (92348). VDRC: UAS-*arm*-RNAi, (7767), UAS-*dsh*-RNAi (101525). upd-Gal4 was kindly gifted from Denise Montell. fz3::RFP was a kind gift from Ramanuj DasGupta. upd::HA was kindly shared by Hiroshi Nakato. We used BDSC #51845 for *cora* knockdown and BDSC #28666 for *nrv2* knockdown if not specified otherwise.

Immunofluorescence staining and imaging

Protocols were carried out at room temperature when not indicated otherwise. Flies were dissected in PBS and ovaries fixed for 20 minutes in 4% PFA. Ovaries were washed thrice for 10 minutes with PBS and blocked for 1h with block solution (PBS with 0,2% Triton X-100 and 0,5% BSA). Primary antibody incubation was performed overnight at 4°C in block solution. For F-actin staining phalloidin (Invitrogen A12380, 1:200) was added to the solution. On the next day the ovaries were washed three times for 10 minutes with block solution and incubated with secondary antibody in block solution for 2-3h. Lastly, ovaries were washed three times for 10 minutes with block solution and twice with PBS. Ovaries were mounted in DAPI Fluoromount-G (ThermoFisher Scientific OB010020).

The following antibodies were used:

DSHB: mouse anti-Cora (1:1000, C566.9), mouse anti-Hts (1:100, 1B1), mouse anti-Fas3 (1:100, 7G10), mouse anti-LamC (1:100, LC28.26), mouse anti-Yan (1:100, 8B12H9), mouse anti-Eya (1:100, 10H6), rat anti-E-Cad (1:50, DCAD2), mouse anti-Dlg1 (1:50, 4F3). Cell Signaling: rabbit anti-c-Dcp1 Asp215 (1:100, #9578), rabbit anti-GFP (1:1000, D5.1). Rabbit anti-HA (1:100, Invitrogen SG77), rat anti-RFP (1:1000, ChromoTek 5F8). Rabbit anti-Baz (1:100, kind gift from Andreas Wodarz), guinea pig anti-zfh1 (1:500, kind gift from James Skeath). Secondary antibodies were purchased from Invitrogen and used at 1:1000: goat anti-guinea pig 488 (A11073), goat anti-mouse 488 (A11029), goat anti-mouse 568 (A11031), goat anti-mouse 647 (A21230), goat anti-rabbit 488 (A11034), goat anti-rabbit 568 (A11036), goat anti-rat 488 (A11006).

For the EdU assay ThermoFisher EdU Alexa Fluor 555 Imaging Kit (C10338) was used. Ovaries were dissected in PBS and incubated in 15 µm EdU in PBS for 1h. Ovaries were washed two times with PBS and fixed for 20 minutes in 4% PFA. Ovaries were blocked for 1h in blocking solution and primary antibody was incubated overnight at 4°C. Ovaries were washed twice with PBS and incubated 30 minutes with Click-iT reaction cocktail and covered. Ovaries were washed two times with PBS and blocked for 1h. Secondary antibody was incubated overnight at 4°C. Ovaries were washed thrice with blocking solution and twice with PBS and mounted in DAPI Fluoromount-G.

Images were acquired with Leica TCS SP8 with HC PL APO CS2 40x/1.30 and HC PL APO CS2 x63/1.4 oil objective and Leica Application Suite X (LasX) software. For intensity measurements images were acquired with the same settings. Image processing, analysis and fluorescence intensity measurements were performed with FIJI 2.9.0 [55]. Dlg1 and Actin colocalization was assessed along the zipper line with the JACoP tool v2.0 from the BIOP plugin in FIJI. Figures were prepared using Inkscape 1.3.2.

EdU positive cell quantification was performed with Imaris 9.3 (Bitplane). Images were imported as z-projections and a region of interest was selected. The total cell count within this region was determined using the DAPI channel spot tool. EdU positive cells were counted within the same region using the RFP channel. Stalk cross-sections were visualized with Imaris 9.3 (Bitplane) using the E-Cad channel of z-stacks taken with 0.75 µm distance.

Statistics and reproducibility

Expression of septate junction components was assessed using a publicly available single cell RNA-sequencing atlas [7] via the DotPlot() function of the Seurat package (5.0.2) in RStudio (2023.12.1+402).

Significance tests were performed with Prism (10) or RStudio (2024.04.0+735). We tested normal distribution with the Shapiro-Wilk test. For normally distributed samples we then performed a student's t-test. For all other samples we performed the Mann-Whitney test. For significance tests of more than two groups we tested for normality and performed the Kruskal-Wallis test. Pearson's Chi-squared test with Yates correction was performed with the chisq.test() command of the stats package (4.3.2) in RStudio (2024.04.0+735). Significance values are reported as: ns > 0.05, * < 0.05, ** < 0.01, *** < 0.001. In box plots, the midline depicts the median, the lower and upper hinges correspond to the 25 and 75 percent quartiles and the whiskers span the smallest and largest values. Quantifications in the main text are reported as arithmetic mean ± SEM.

All images and quantifications are representatives of at least 3 technical and 15 biological replicates.

Data availability

The data that support the findings of this study are available within the article, Supplementary Information, or from the corresponding author upon request.

References

1. Sahai-Hernandez, P. & Nystul, T. G. A dynamic population of stromal cells contributes to the follicle stem cell niche in the Drosophila ovary. *Development* **140**, 4490–4498 (2013).
2. Song, X. & Xie, T. Wingless signaling regulates the maintenance of ovarian somatic stem cells in Drosophila. *Development* **130**, 3259–3268 (2003).
3. Forbes, A. J., Lin, H., Ingham, P. W. & Spradling, A. C. hedgehog is required for the proliferation and specification of ovarian somatic cells prior to egg chamber formation in Drosophila. *Development* **122**, 1125–1135 (1996).
4. Wang, X. & Page-McCaw, A. A matrix metalloproteinase mediates long-distance attenuation of stem cell proliferation. *J. Cell Biol*. **206**, 923–936 (2014).
5. Dai, W., Peterson, A., Kenney, T., Burrous, H. & Montell, D. J. Quantitative microscopy of the Drosophila ovary shows multiple niche signals specify progenitor cell fate. *Nat. Commun*. **8**, 1244 (2017).
6. Assa-Kunik, E., Torres, I. L., Schejter, E. D., Johnston, D. S. & Shilo, B.-Z. Drosophila follicle cells are patterned by multiple levels of Notch signaling and antagonism between the Notch and JAK/STAT pathways. *Development* **134**, 1161–1169 (2007).
7. Rust, K. et al. A single-cell atlas and lineage analysis of the adult Drosophila ovary. *Nat. Commun*. **11**, 5628 (2020).
8. Rust, K. & Nystul, T. Signal transduction in the early Drosophila follicle stem cell lineage. *Current Opinion in Insect Science* **37**, 39–48 (2020).
9. McGregor, J. R., Xi, R. & Harrison, D. A. JAK signaling is somatically required for follicle cell differentiation in Drosophila. *Development* **129**, 705–717 (2002).
10. Franz, A. & Riechmann, V. Stepwise polarisation of the Drosophila follicular epithelium. *Dev. Biol*. **338**, 136–147 (2010).
11. Müller, H. A. Genetic control of epithelial cell polarity: lessons from Drosophila. *Dev. Dyn*. **218**, 52–67 (2000).
12. Izumi, Y. & Furuse, M. Molecular organization and function of invertebrate occluding junctions. *Semin. Cell Dev. Biol.* **36**, 186–193 (2014).
13. Rice, C., De, O., Alhadyian, H., Hall, S. & Ward, R. E. Expanding the Junction: New Insights into Non-Occluding Roles for Septate Junction Proteins during Development. *J Dev Biol* **9**, (2021).
14. Nelson, K. S., Furuse, M. & Beitel, G. J. The Drosophila Claudin Kune-kune is required for septate junction organization and tracheal tube size control. *Genetics* **185**, 831–839 (2010).
15. Baumgartner, S. et al. A Drosophila neurexin is required for septate junction and blood-nerve barrier formation and function. *Cell* **87**, 1059–1068 (1996).
16. Banerjee, S. et al. A Laminin G-EGF-Laminin G module in Neurexin IV is essential for the apico-lateral localization of Contactin and organization of septate junctions. *PLoS One* **6**, e25926 (2011).
17. Lamb, R. S., Ward, R. E., Schweizer, L. & Fehon, R. G. Drosophila coracle, a member of the protein 4.1 superfamily, has essential structural functions in the septate junctions and developmental functions in embryonic and adult epithelial cells. *Mol. Biol. Cell* **9**, 3505–3519 (1998).
18. Fehon, R. G., Dawson, I. A. & Artavanis-Tsakonas, S. A Drosophila homologue of membrane-skeleton protein 4.1 is associated with septate junctions and is encoded by the coracle gene. *Development* **120**, 545–557 (1994).
19. Paul, S. M., Ternet, M., Salvaterra, P. M. & Beitel, G. J. The Na+/K+ ATPase is required for septate junction function and epithelial tube-size control in the Drosophila tracheal system. *Development* **130**, 4963–4974 (2003).
20. Paul, S. M., Palladino, M. J. & Beitel, G. J. A pump-independent function of the Na,K-ATPase is required for epithelial junction function and tracheal tube-size control. *Development* **134**,

147–155 (2007).
21. Banerjee, S., Sousa, A. D. & Bhat, M. A. Organization and function of septate junctions: an evolutionary perspective. *Cell Biochem. Biophys*. **46**, 65–77 (2006).
22. Alhadyian, H., Shoaib, D. & Ward, R. E. Septate junction proteins are required for egg elongation and border cell migration during oogenesis in Drosophila. *G3* **11**, (2021).
23. Rouka, E. et al. The Drosophila septate junctions beyond barrier function: Review of the literature, prediction of human orthologs of the SJ-related proteins and identification of protein domain families. *Acta Physiol.* **231**, e13527 (2021).
24. Alhadyian, H., Shoaib, D. & Ward, R. E. Septate junction proteins are required for egg elongation and border cell migration during oogenesis in Drosophila. *G3* **11**, (2021).
25. Felix, M., Chayengia, M., Ghosh, R., Sharma, A. & Prasad, M. Pak3 regulates apical-basal polarity in migrating border cells during Drosophila oogenesis. *Development* **142**, 3692–3703 (2015).
26. Hartman, R. et al. Novel Tools for Genetic Manipulation of Follicle Stem Cells in the Drosophila Ovary Reveal an Integrin-Dependent Transition from Quiescence. *Genetics* **199**, 935–957 (2015).
27. Tiklová, K., Senti, K.-A., Wang, S., Gräslund, A. & Samakovlis, C. Epithelial septate junction assembly relies on melanotransferrin iron binding and endocytosis in Drosophila. *Nat. Cell Biol.* **12**, 1071–1077 (2010).
28. Izumi, Y., Furuse, K. & Furuse, M. Septate junctions regulate gut homeostasis through regulation of stem cell proliferation and enterocyte behavior in Drosophila. *J. Cell Sci.* **132**, (2019).
29. Chen, H.-J., Li, Q., Nirala, N. K. & Ip, Y. T. The Snakeskin-Mesh Complex of Smooth Septate Junction Restricts Yorkie to Regulate Intestinal Homeostasis in Drosophila. *Stem Cell Reports* **14**, 828–844 (2020).
30. Ward, R. E., 4th, Schweizer, L., Lamb, R. S. & Fehon, R. G. The protein 4.1, ezrin, radixin, moesin (FERM) domain of Drosophila Coracle, a cytoplasmic component of the septate junction, provides functions essential for embryonic development and imaginal cell proliferation. *Genetics* **159**, 219–228 (2001).
31. Boisclair Lachance, J.-F. et al. A comparative study of Pointed and Yan expression reveals new complexity to the transcriptional networks downstream of receptor tyrosine kinase signaling. *Dev. Biol*. **385**, 263–278 (2014).
32. Pearson, J. R. et al. ECM-Regulator timp Is Required for Stem Cell Niche Organization and Cyst Production in the Drosophila Ovary. *PLoS Genet.* **12**, e1005763 (2016).
33. Bai, J. & Montell, D. Eyes absent, a key repressor of polar cell fate during Drosophila oogenesis. *Development* **129**, 5377–5388 (2002).
34. Borensztejn, A., Mascaro, A. & Wharton, K. A. JAK/STAT signaling prevents excessive apoptosis to ensure maintenance of the interfollicular stalk critical for Drosophila oogenesis. *Dev. Biol*. **438**, 1–9 (2018).
35. Nystul, T. G. & Spradling, A. An Epithelial Niche in the Drosophila Ovary Undergoes Long-Range Stem Cell Replacement. *Cell Stem Cell* **1**, 277–285 (2007).
36. Laprise, P. et al. Yurt, Coracle, Neurexin IV and the Na(+),K(+)-ATPase form a novel group of epithelial polarity proteins. *Nature* **459**, 1141–1145 (2009).
37. De, O., Rice, C., Zulueta-Coarasa, T., Fernandez-Gonzalez, R. & Ward, R. E., 4th. Septate junction proteins are required for cell shape changes, actomyosin reorganization and cell adhesion during dorsal closure in Drosophila. *Front Cell Dev Biol* **10**, 947444 (2022).
38. Van De Bor, V. et al. A dynamic and mosaic basement membrane controls cell intercalation in Drosophila ovaries. *Development* **148**, (2021).
39. Ghiglione, C. et al. The Drosophila cytokine receptor Domeless controls border cell migration and epithelial polarization during oogenesis. *Development* **129**, 5437–5447 (2002).
40. Niewiadomska, P., Godt, D. & Tepass, U. DE-Cadherin is required for intercellular motility

during Drosophila oogenesis. *J. Cell Biol.* **144**, 533–547 (1999).
41. Campanale, J. P., Mondo, J. A. & Montell, D. J. A Scribble/Cdep/Rac pathway controls follower-cell crawling and cluster cohesion during collective border-cell migration. *Dev. Cell* **57**, 2483–2496.e4 (2022).
42. Wu, J., Klein, T. J. & Mlodzik, M. Subcellular localization of frizzled receptors, mediated by their cytoplasmic tails, regulates signaling pathway specificity. *PLoS Biol.* **2**, E158 (2004).
43. Wang, Y., Guo, N. & Nathans, J. The role of Frizzled3 and Frizzled6 in neural tube closure and in the planar polarity of inner-ear sensory hair cells. *J. Neurosci.* **26**, 2147–2156 (2006).
44. Castanieto, A., Johnston, M. J. & Nystul, T. G. EGFR signaling promotes self-renewal through the establishment of cell polarity in Drosophila follicle stem cells. *Elife* **3**, (2014).
45. Song, X. & Xie, T. DE-cadherin-mediated cell adhesion is essential for maintaining somatic stem cells in the Drosophila ovary. *Proceedings of the National Academy of Sciences* **99**, 14813–14818 (2002).
46. Bergstralh, D. T., Lovegrove, H. E. & St Johnston, D. Lateral adhesion drives reintegration of misplaced cells into epithelial monolayers. *Nat. Cell Biol.* **17**, 1497–1503 (2015).
47. Alégot, H., Pouchin, P., Bardot, O. & Mirouse, V. Jak-Stat pathway induces Drosophila follicle elongation by a gradient of apical contractility. *Elife* **7**, (2018).
48. Chen, H.-J. et al. The Hippo pathway controls polar cell fate through Notch signaling during Drosophila oogenesis. *Dev. Biol.* **357**, 370–379 (2011).
49. Carvalho, L. et al. Occluding junctions as novel regulators of tissue mechanics during wound repair. *J. Cell Biol.* **217**, 4267–4283 (2018).
50. Faivre-Sarrailh, C. Molecular organization and function of vertebrate septate-like junctions. *Biochim. Biophys. Acta Biomembr*. **1862**, 183211 (2020).
51. Shin, K., Fogg, V. C. & Margolis, B. Tight junctions and cell polarity. *Annu. Rev. Cell Dev. Biol.* **22**, 207–235 (2006).
52. Nehme, Z., Roehlen, N., Dhawan, P. & Baumert, T. F. Tight junction protein signaling and cancer biology. *Cells* **12**, 243 (2023).
53. Xu, C. et al. The Septate Junction Protein Tsp2A Restricts Intestinal Stem Cell Activity via Endocytic Regulation of aPKC and Hippo Signaling. *Cell Rep.* **26**, 670–688.e6 (2019).
54. Khadilkar, R. J. & Tanentzapf, G. Septate junction components control Drosophila hematopoiesis through the Hippo pathway. *Development* **146**, (2019).
55. Schindelin, J. et al. Fiji: an open-source platform for biological-image analysis. *Nat. Methods* **9**, 676–682 (2012).

Acknowledgements

We thank the Bloomington Stock center and Denise Montell for fly stocks and Andreas Wodarz and James Skeath for kindly gifted antibodies. We are grateful to Sona Martirosan for the initial assessment of phenotypes caused by stalk and polar cell specific knockdown of septate junction components. We thank Andreas Wodarz, Sven Bogdan and Dennis Klug for constructive comments on the manuscript. This work was supported by the PSI (Promoting Scientific Independence) Program of the Philipps-University Marburg.

Author contributions

K.R. designed the project and wrote the manuscript. V.H. and K.R. made the figures. A.S und V.H. performed dissections and immunofluorescence stainings. V.H. performed microscopy, quantifications and statistical analyses. All authors commented on the manuscript.

Competing interests

The authors declare no competing interests.

Figures

Figure 1:

a) Graphic representation of the *Drosophila* ovary and the early stages of oogenesis. TF: terminal filament, CC: cap cell, GSC: germline stem cell, GC: germ cell, EC: escort cell, a: anterior, c: central, p: posterior, FSC: follicle stem cell, pFC: prefollicle cell, MB: main body follicle cell, PC: polar cell, SC: stalk cell. Inset on the right highlights the apical to basal orientation of main body follicle cells. b) Average and percent expression of septate junction core components and tricellular septate junction (tSJ) components in escort cells and early follicle cell types identified in [7]. Many septate junction components display high expression in polar cells and several components are enriched in escort cells. c) Germarium and early cyst stages stained for Nrx-IV::mCherry (magenta) and DAPI (blue). Nrx-IV::mCherry is highly expressed in escort cells (EC) and polar cells (arrowheads). d) Wildtype ovariole (109-30^{ts} > *w*^{1118}) stained for Cora. Cora is expressed in escort cells and follicle cells with high expression in mature stalk (arrow). e-i) Immunostaining (e-f) and associated quantification (i) of Cora staining in Stage 6 main body follicle. 109-30^{ts} was used to induce the respective RNAi. In wildtype Cora mostly localizes laterally. Knockdown of *nrv2*, *Nrx-IV* or *kune* disturbs normal Cora localization. Label in e) illustrates how we divided the lateral membrane into the apical ("a"), lateral ("l") and basal ("b") portions. i) n = 6, 7, 7, 6 measurements for each condition. j-l) Germaria of the indicated genotype stained for DAPI (blue) and the follicle cell marker Fas3 (green or white in j'-l'). Germline cysts encapsulated by follicle cells in the germarium are marked by asterisks. m) Quantification of cysts in Region 2b in 109-30^{ts} crossed with the respective genotype. n = 37, 22, 21, 36, 42, 14, 15 germaria respectively. n-p) Stalk regions of the genotypes indicated in each respective row stained for Hts. Note that wildtype stalk forms a single row of cells (n) while knockdown of septate junction components results in double rowed stalks (o-p). q) Quantification of cells per stalk (Stage 4) in ovarioles from 109-30^{ts} crossed to the respective allele. n = 28, 11, 9, 12, 6, 28, 12 stalks respectively.

Figure 2:

a-b) Quantification of the percentage of proliferating cells in Region 2b (a) or main body follicle cells of Stage 5-6 cysts (b) in ovarioles of 109-30^{ts} crossed to the respective allele. a) n = 10, 11, 10, 12, 11, 11, 15 germaria. b) n ≥ 9, 11, 9, 8, 10, 11, 13 ovarioles. c-e) Germaria of 109-30^{ts} crossed to fz3::RFP and the respective allele and stained for DAPI (blue), RFP (magenta) and Fas3 (white). c'-e') show the RFP channel in white. Yellow dotted line shows the Fas3 border

between Region 2a and 2b. f) Associated quantification of fz3::RFP intensity in Region 2b for genotypes shown in (c-e). n = 8, 9, 6 germaria respectively. g-i) Ovarioles of the 109-30^{ts} driver crossed to the wildtype *w*^{1118} (g), *arm*-RNAi (h) or *dsh*-RNAi (i) and stained for DAPI (blue) and Fas3 (green). g'-i') show Fas3 in white. Asterisks mark Region 2b cysts. j) Quantification of cysts in Region 2b in the wildtype (109-30^{ts} > *w*^{1118}) or upon reduction of Wnt signaling by RNAi depletion of *arm* or *dsh* in follicle cells with 109-30^{ts}. n = 26, 21, 18 germaria respectively. k-m) Ovarioles of the respective genotypes stained for DAPI (blue) and zfh1 (magenta). Insets are magnified in k'-m') and show zfh1 staining (white) in the second stalk. n-v) First stalks of ovarioles of the genotype indicated in the respective row stained for DAPI and for a cell type specific marker (green): aop (n-p), LamC (q-s), eya (t-v).

Figure 3:

a-f) Consecutive stages of stalk morphogenesis in wildtype ovaries of the genotype 109-30^{ts} > *w*^{1118} stained for E-Cad (a-f) and Phalloidin (a'-f'). A graphic representation of stalk morphogenesis is depicted in g). h-j) Snapshots of live imaging analysis of E-Cad-3xGFP during stalk morphogenesis from the budding stage (h) to the first stalk (i). j) Snapshots of a maximum intensity projection in 30 minute intervals. Yellow dotted line marks the stalk region.

Figure 4:

a-c) Imaris analysis of E-Cad expression in ovarioles from 109-30^{ts} crossed to the indicated genotype. Cross-sections (right) are labeled in the maximum intensity overview (left). Yellow dotted line outlines the stalk diameter. d-f) Budding stalk regions of ovarioles from 109-30^{ts} crossed to the allele indicated in each row stained for E-Cad (green) and Baz (magenta) (d-f) or E-Cad (d'-f') or Baz (d"-f") in white. Arrows indicate regions of apical membrane lacking E-Cad and Baz staining. g-h) Quantification of E-Cad (g) and Baz (h) staining across the zipper line in Region 3 intercalating stalks of 109-30^{ts} crossed to the respective allele. n = 5, 4, 4, 4, 5, 5, 4 ovarioles respectively for g) and h). i-k) Budding stalk regions of 109-30^{ts} crossed to the indicated genotype stained for Dlg (green) and Phalloidin (magenta) (i-k) or Dlg (i'-k') or Phalloidin (i"-k") in white. Arrowheads indicate regions with co-localization of Dlg and F-actin along the apical membrane. l) Pearson's coefficient describing the colocalization of Dlg and F-actin along the apical zipper line. n = 6, 8, 7, 6, 7, 6, 6 respectively. m) Quantification of basal to apical Phalloidin staining in budding stalk cells in 109-30^{ts} crossed to the respective genotype. n = 11, 15, 9, 14, 18, 16, 17 ovarioles respectively.

Figure 5:

a-c) Ovarioles of the wildtype (a) or with stalk cell specific knockdown of *cora* (b) or *nrv2* (c) stained for DAPI (blue) and LamC (green). Insets are enlarged on the right and show LamC staining (white) in the second stalk. d) Quantification of cells per Stage 4 stalk in ovarioles of CG46339^{ts} crossed to the respective genotype. Stalk cell specific knockdown of septate junction components does not significantly increase stalk cell numbers or leads to only a mild increase. n = 9, 5, 5, 5, 5, 5, 5 stalks respectively. e-g) Ovarioles of the wildtype (e) or with polar cells specific knockdown of *cora* (f) or *nrv2* (g) stained for DAPI (blue) and LamC (green). Insets on the right show the second stalk stained for LamC (white). h) Quantification of cells per stalk (Stage 4) in ovarioles with upd^{ts} crossed to the respective genotype. n = 8, 8, 8, 8, 10, 6 stalks respectively. i-k) Ovarioles of 109-30^{ts} combined with the Jak-STAT reporter UAS-2xSTAT-eGFP and the respective allele as indicated. We stained for DAPI (blue), GFP (green) and Fas3 (white) (i-k). i'-k') show the 2xSTAT-GFP channel (white). Insets on the right show the first or second stalk as indicated and stained for DAPI (blue), GFP (green) and Fas3 (white) on the left or 2xSTAT-GFP (white) on the right. l) Quantification of 2xSTAT-GFP in Region 2b, early stalk or mature stalk cells in 109-30^{ts} crossed to the respective genotype. n = 6, 5, 5, 14, 14, 14, 14, 14, 14 ovarioles respectively.

Figure 6:

a) A germline cyst expressing Upd1::HA stained for HA (magenta), Fas3 (green) and DAPI (blue) and insets showing the indicated channels. Green line indicates the apical cap region in the Fas3 channel. Yellow outline in the DAPI channel marks the epithelium. b) Polar cells of ovarioles of 109-30^{ts} crossed to the indicated genotype and stained for E-Cad, Fas3, Phalloidin and DAPI as indicated (white). Apical side facing the germline cyst is oriented towards the bottom. The epithelium is outlined by a yellow dotted line in the DAPI channel. Note the presence of the apical cap in both examples of wildtype polar cells marked by a green line. c) Graphical overview of a polar cell cluster with apical cap and apical Upd1 enrichment. d) Quantification of Fas3 intensity of the apical polar cell membrane to apical main body follicle cell side in ovarioles of 109-30^{ts} crossed to the indicated genotype. n = 16, 20, 16, 18, 20, 18, 20 ovarioles respectively. e) Graph summarizing the functions of septate junction core components in early follicle cell development. Septate junctions allow normal FSC/pFC proliferation rates by promoting Wnt signaling activity which is vital for effective cyst encapsulation in Region 2b. Septate junctions further regulate stalk morphogenesis non-cell-autonomously by maintaining cell polarity in polar cells and thereby fine-

tuning Jak-STAT signaling activity. Additionally, they cell-autonomously control stalk cell apical-basal polarity, cell adhesion and actin cytoskeleton to coordinate the intercalation process.

Supplementary Figure 1

a) Ovariole expressing RedStinger (magenta) under the 109-30-Gal4 driver and stained for Fas3 (green) and DAPI (blue). a') RedStinger expression in white. b-c) Ovarioles of 109-30^{ts} crossed to *w*^{1118} (b) or *cora*-RNAi (c) and stained for Cora. d-e) Ovarioles with pan-follicle cell depletion of *Nrx-IV* (d) or *kune* (e) stained for DAPI (blue) and Fas3 (green). f) Quantification of the frequency of ovarioles with more than two germline cysts in Region 2b of 109-30^{ts} crossed to the respective allele. For control genotypes the CyO positive sibling flies, which lack the 109-30-Gal4 allele, were dissected. P-values from Chi-squared test. n = 247, 236, 184, 219, 154, 232, 161, 252, 153, 150, 134, 158, 142 germaria respectively. g) Quantification of the stage of the second budded cyst in ovarioles with 109-30^{ts} driving the indicated allele. For significance testing we used stage numbers as values. n = 9, 10, 14, 12, 14, 11, 14 ovarioles respectively. h-i) Stalk regions of ovarioles of 109-30^{ts} crossed to *Nrx-IV*-RNAi (h) or *kune*-RNAi (i) stained for Hts. j) Quantification of the frequency of ovarioles with double row stalk (Stage 4 or later) of 109-30^{ts} crossed to the respective allele. Control flies were devoid of 109-30-Gal4. P-values from Chi-squared test. n = 197, 138, 149, 140, 135, 140, 136, 148, 144, 142, 133, 140, 147 ovarioles respectively.

Supplementary Figure 2

a-e) Ovarioles of the respective genotypes stained for DAPI (blue) and EdU (magenta). Stalk cells are EdU negative and outlined in yellow. f-m) Immunostainings of ovarioles of 109-30^{ts} driving *Nrx-IV*-RNAi (f, h, j, l) or *kune*-RNAi (g, i, k, m) stained for DAPI (blue) and zfh1 (magenta) (f-g) with an inset showing zfh1 staining in white in the second stalk (f'-g'), or second stalks stained for DAPI (blue) and a cell type specific marker in green: aop (h-i), LamC (j-k) or eya (l-m). n) 109-30^{ts} > *w*^{1118} ovariole stained for DAPI (blue), c-Dcp-1 (green) and Fas3 (white). n') shows c-Dcp-1 (white). We detected c-Dcp-1 staining in Fas3 high polar cells but not in stalk cells. o) Quantification of Fas3 staining in ovarioles from 109-30^{ts} crossed to the respective allele. Fas3 intensity in Stage 4 stalk cells was normalized to Fas3 intensity in Region 2b follicle cells to circumvent influence of staining differences. n = 6, 7, 7, 7, 7, 7, 7 stalks respectively.

Supplementary Figure 3

a-f) Immunostainings of consecutive stages of stalk development of 109-30^{ts} crossed to *w*^{1118} stained for E-Cad (a-f), Cora (a'-f') and Phalloidin (a"-f") in white. g-h) Maximum intensity

projections and stalk cross sections of E-Cad staining in 109-30^{ts} driving *Nrx-IV*-RNAi (g) or *kune*-RNAi (h). i-l) Immunostainings of budding stalk regions of 109-30^{ts} driving *Nrx-IV*-RNAi (i, k) or *kune*-RNAi (j, l) stained for E-Cad and Baz (i-j) or Dlg and Phalloidin (k-l) as indicated. m) Ovariole with pan-follicle cell depletion of *E-Cad* (109-30^{ts} driving *E-Cad*-RNAi) stained for Fas3 (green) and DAPI (blue). Areas with cyst fusion and double row stalks are outlined in yellow.

Supplementary Figure 4

a-b) Ovarioles of the stalk cell driver CG46339^{ts} driving *Nrx-IV*-RNAi (a) or *kune*-RNAi (b) stained for DAPI (blue) and LamC (green). Insets of the second stalk on the right show LamC in white. c-g) Ovarioles of CG46339^{ts} driving the indicated genotype stained for DAPI (blue) and Fas3 (green). Insets on the right show the second stalk stained for Fas3 (white). h) Quantification of the frequency of CG46339^{ts} ovarioles crossed to the respective allele with double row stalks (Stage 4 or older). P-values from Chi-squared test. n = 196, 150, 194, 180, 154, 135, 135 ovarioles respectively. i) Immunostaining for DAPI (blue) and LamC (green) of an ovariole expressing *Nrx-IV*-RNAi under the upd^{ts} driver. LamC staining of the second stalk region is shown in white in the inset. j-m) Ovarioles of upd^{ts} driving the indicated genotype and stained for DAPI (blue) and Fas3 (green). Insets on the right show the second stalk and Fas3 staining in white. Please note that the knockdown of *kune* with upd^{ts} was lethal. n) Quantification of the frequency of ovarioles with double row stalks (Stage 4 or later) of upd^{ts} crossed to the respective genotype. n = 31, 56, 64, 62, 54, 35 ovarioles respectively. o) Quantification of 2xSTAT intensity in the three main body follicle cells neighboring anterior polar cells in Stage 5-6 follicles in the background of 109-30^{ts} driving the indicated genotype. n = 5 ovarioles for each condition.

Supplementary Figure 5

a) Polar cells in ovarioles of 109-30^{ts} driving *Nrx-IV*-RNAi (upper panel) or *kune*-RNAi (lower panel) stained for E-Cad, Fas3, Phalloidin and DAPI as indicated. The follicle epithelium is outlined in the DAPI channel. Apical side facing the germline cyst is located on the bottom. b-c) Quantification of the ratio of F-actin (b) and E-Cad (c) of the apical side of the polar cell to apical side of the neighboring main body follicle cells of 109-30^{ts} crossed to the respective genotype. n = 16, 20, 16, 18, 20, 18, 20 ovarioles for the genotypes respectively for b) and c).

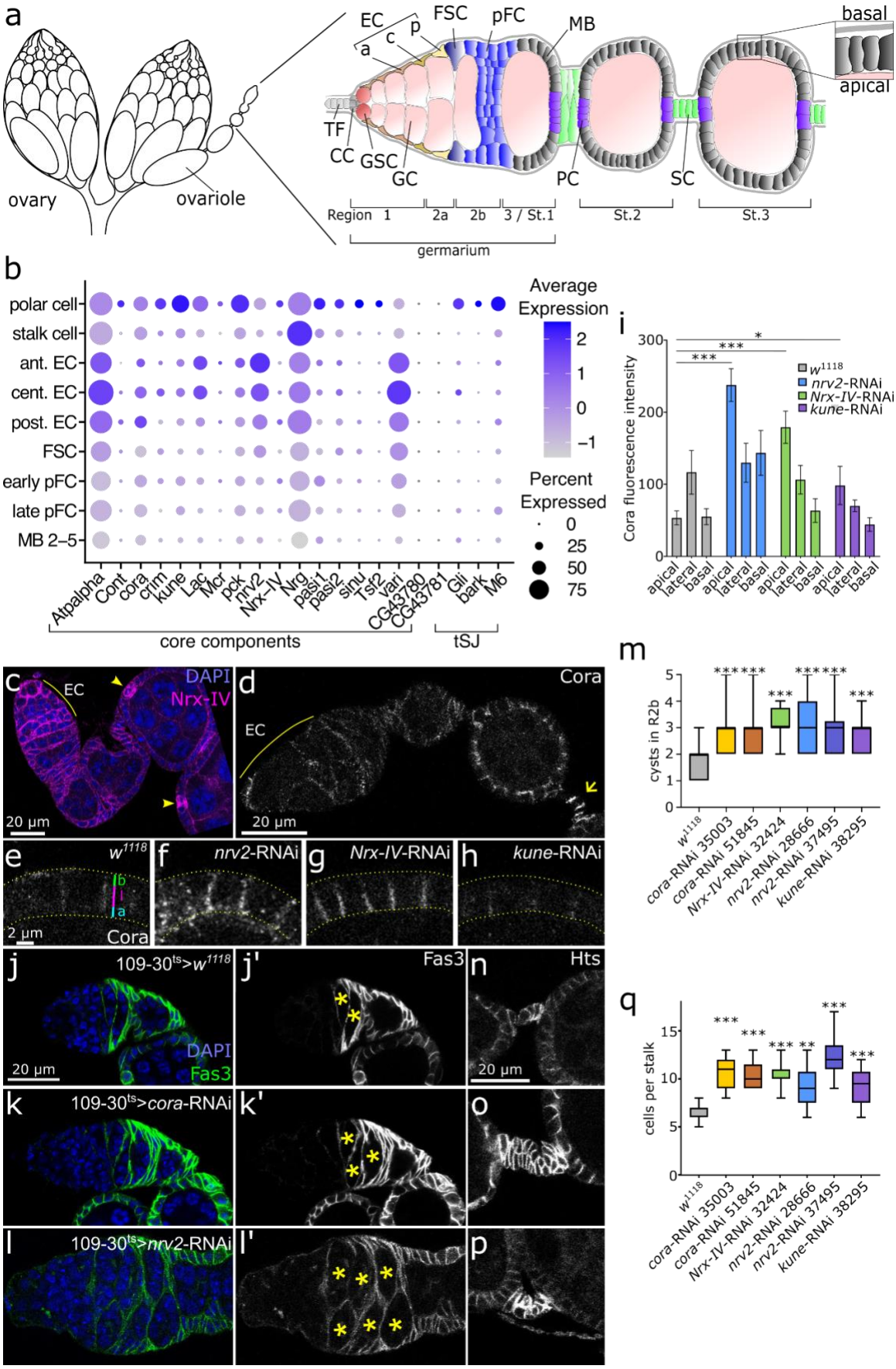
a
ovary
ovariole
EC
c
p
a
FSC
pFC
MB
basal
apical
TF
CC
GSC
GC
PC
SC
Region 1
2a
2b
3 / St.1
St.2
St.3
germarium
b
polar cell
stalk cell
ant. EC
cent. EC
post. EC
FSC
early pFC
late pFC
MB 2–5
Atpalpha
Cont
cora
crim
kune
Lac
Mcr
pck
nrv2
Nrx-IV
Nrg
pasi1
pasi2
sinu
Tsf2
vari
CG43780
CG43781
Gli
bark
M6
core components
tSJ
Average Expression
Percent Expressed
i
Cora fluorescence intensity
w1118
nrv2-RNAi
Nrx-IV-RNAi
kune-RNAi
apical
lateral
basal
c
DAPI
Nrx-IV
EC
20 µm
d
Cora
e
w1118
2 µm
f
nrv2-RNAi
g
Nrx-IV-RNAi
h
kune-RNAi
j
109-30ts>w1118
DAPI
Fas3
j'
k
109-30ts>cora-RNAi
k'
l
109-30ts>nrv2-RNAi
l'
n
Hts
o
p
m
cysts in R2b
cora-RNAi 35003
cora-RNAi 51845
Nrx-IV-RNAi 32424
nrv2-RNAi 28666
nrv2-RNAi 37495
kune-RNAi 38295
q
cells per stalk

Figure 1

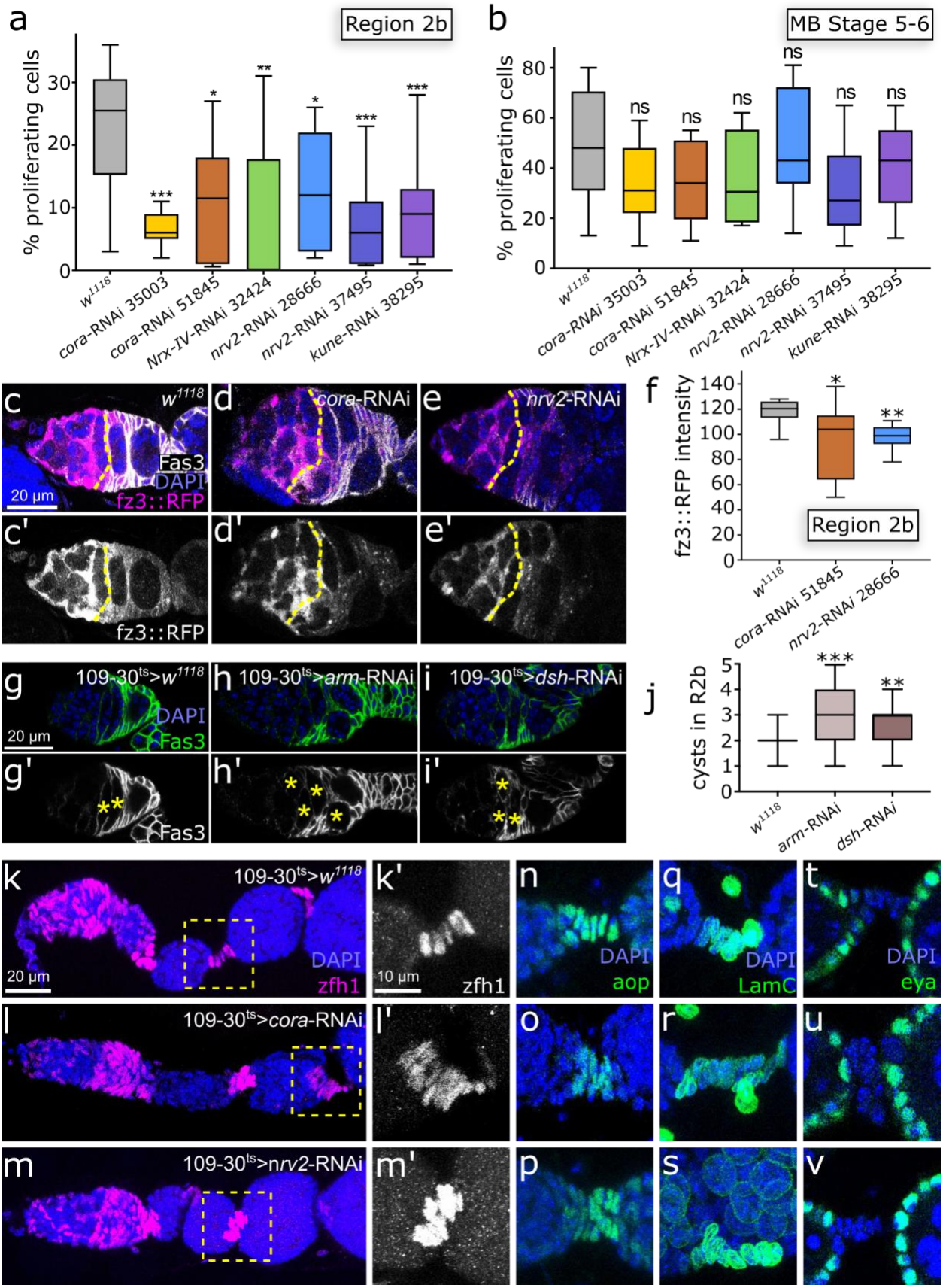
a
Region 2b
% proliferating cells
0
10
20
30
***
*
**
*
***
***
w1118
cora-RNAi 35003
cora-RNAi 51845
Nrx-IV-RNAi 32424
nrv2-RNAi 28666
nrv2-RNAi 37495
kune-RNAi 38295
b
MB Stage 5-6
% proliferating cells
0
20
40
60
80
ns
ns
ns
ns
ns
ns
ns
w1118
cora-RNAi 35003
cora-RNAi 51845
Nrx-IV-RNAi 32424
nrv2-RNAi 28666
nrv2-RNAi 37495
kune-RNAi 38295
c
w1118
Fas3
DAPI
fz3::RFP
20 µm
d
cora-RNAi
e
nrv2-RNAi
c'
fz3::RFP
d'
e'
f
fz3::RFP intensity
0
20
40
60
80
100
120
140
*
**
Region 2b
w1118
cora-RNAi 51845
nrv2-RNAi 28666
g
109-30ts>w1118
DAPI
Fas3
20 µm
h
109-30ts>arm-RNAi
i
109-30ts>dsh-RNAi
g'
Fas3
h'
i'
j
cysts in R2b
0
1
2
3
4
5
***
**
w1118
arm-RNAi
dsh-RNAi
k
109-30ts>w1118
DAPI
zfh1
20 µm
k'
10 µm
zfh1
n
DAPI
aop
q
DAPI
LamC
t
DAPI
eya
l
109-30ts>cora-RNAi
l'
o
r
u
m
109-30ts>nrv2-RNAi
m'
p
s
v

Figure 2

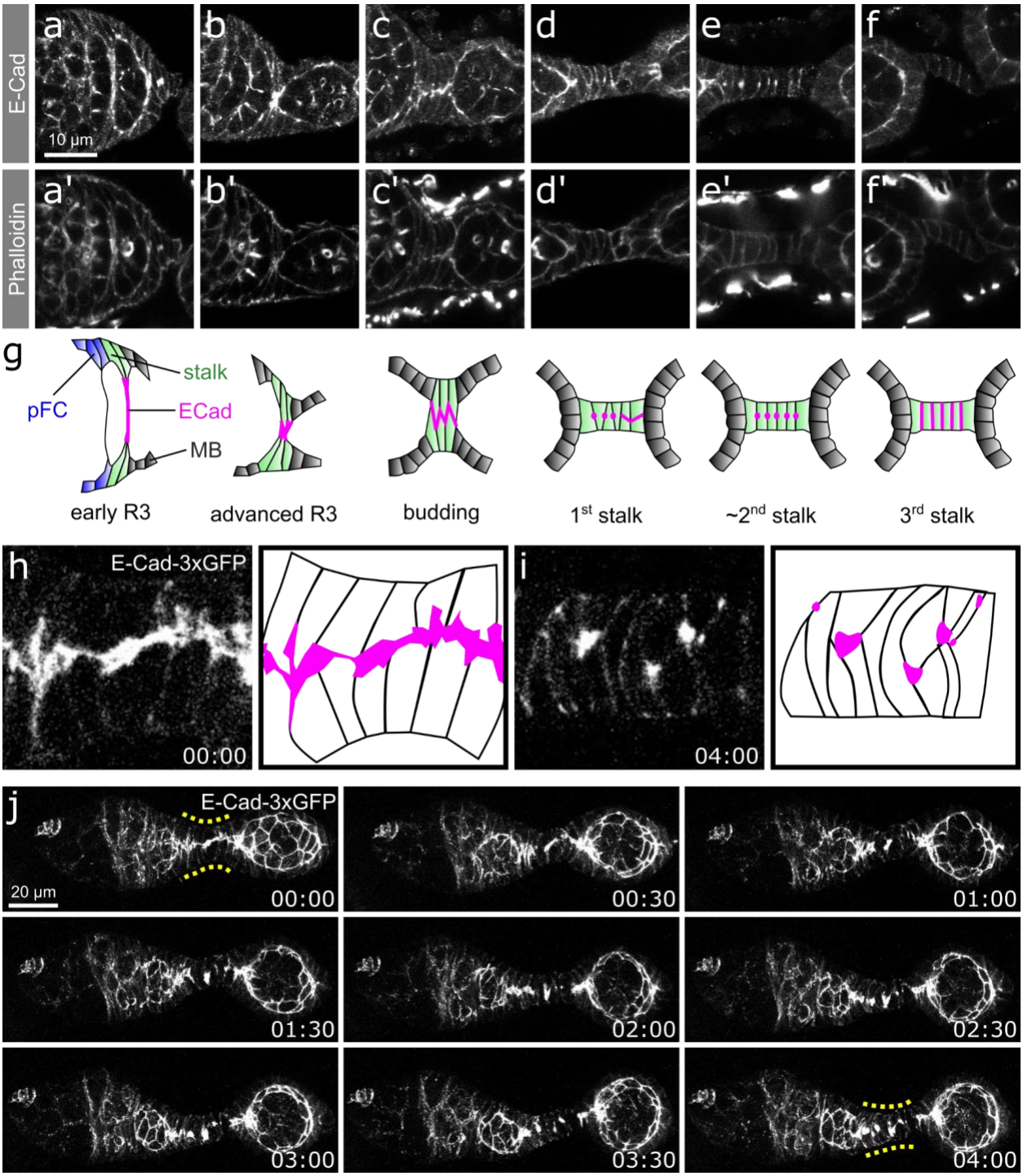
E-Cad
Phalloidin
a
b
c
d
e
f
a'
b'
c'
d'
e'
f'
10 µm
g
stalk
pFC
ECad
MB
early R3
advanced R3
budding
1st stalk
~2nd stalk
3rd stalk
h
E-Cad-3xGFP
00:00
i
04:00
j
E-Cad-3xGFP
20 µm
00:00
00:30
01:00
01:30
02:00
02:30
03:00
03:30
04:00

Figure 3

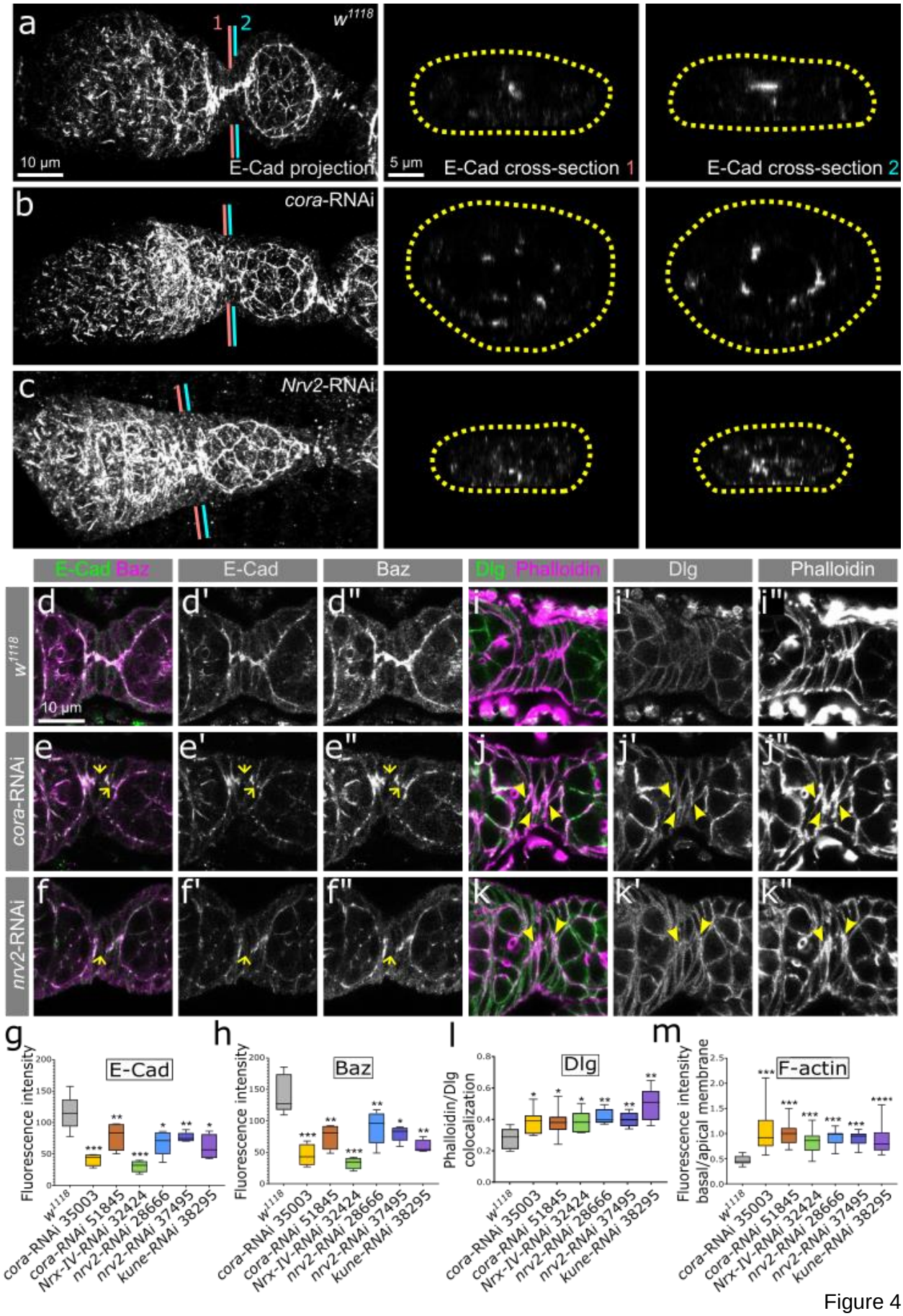
a
1
2
w1118
10 µm
E-Cad projection
5 µm
E-Cad cross-section 1
E-Cad cross-section 2
b
cora-RNAi
c
Nrv2-RNAi
E-Cad Baz
E-Cad
Baz
Dlg Phalloidin
Dlg
Phalloidin
w1118
cora-RNAi
nrv2-RNAi
d
d'
d''
i
i'
i''
e
e'
e''
j
j'
j''
f
f'
f''
k
k'
k''
g
E-Cad
Fluorescence intensity
h
Baz
Fluorescence intensity
i
Dlg
Phalloidin/Dlg colocalization
m
F-actin
Fluorescence intensity basal/apical membrane
w1118
cora-RNAi 35003
cora-RNAi 51845
Nrx-IV-RNAi 32424
nrv2-RNAi 28666
nrv2-RNAi 37495
kune-RNAi 38295

Figure 4

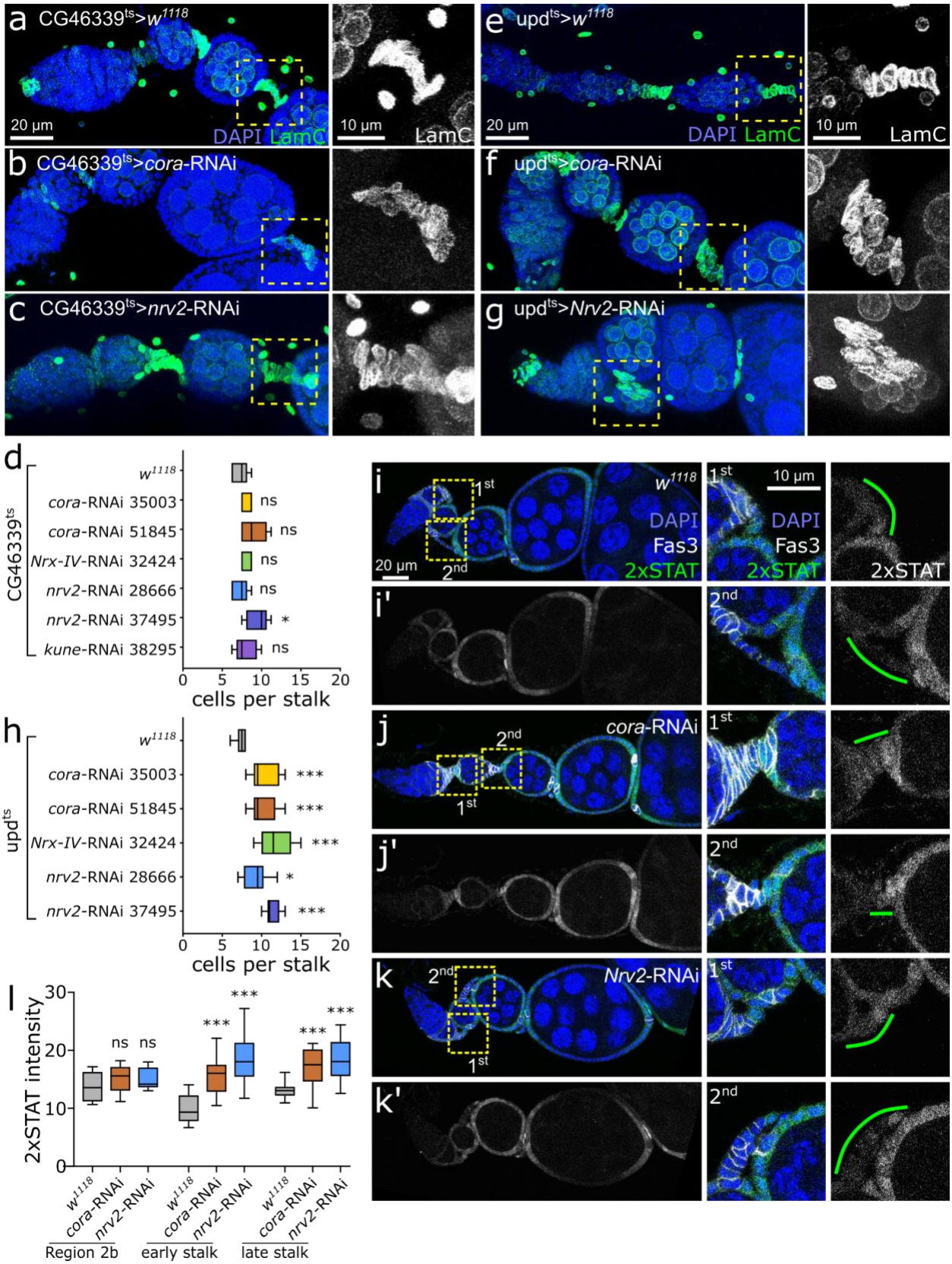
a CG46339ts>w1118
20 µm
DAPI LamC
10 µm
LamC
e updts>w1118
20 µm
DAPI LamC
10 µm
LamC
b CG46339ts>cora-RNAi
f updts>cora-RNAi
c CG46339ts>nrv2-RNAi
g updts>Nrv2-RNAi
d
CG46339ts
w1118
cora-RNAi 35003
cora-RNAi 51845
Nrx-IV-RNAi 32424
nrv2-RNAi 28666
nrv2-RNAi 37495
kune-RNAi 38295
ns
*
0 5 10 15 20
cells per stalk
h
updts
w1118
cora-RNAi 35003
cora-RNAi 51845
Nrx-IV-RNAi 32424
nrv2-RNAi 28666
nrv2-RNAi 37495
***
*
0 5 10 15 20
cells per stalk
i
w1118
1st
2nd
20 µm
DAPI
Fas3
2xSTAT
10 µm
i'
j
cora-RNAi
j'
k
Nrv2-RNAi
k'
l
2xSTAT intensity
0 10 20 30
ns ns
***
w1118
cora-RNAi
nrv2-RNAi
Region 2b
early stalk
late stalk

Figure 5

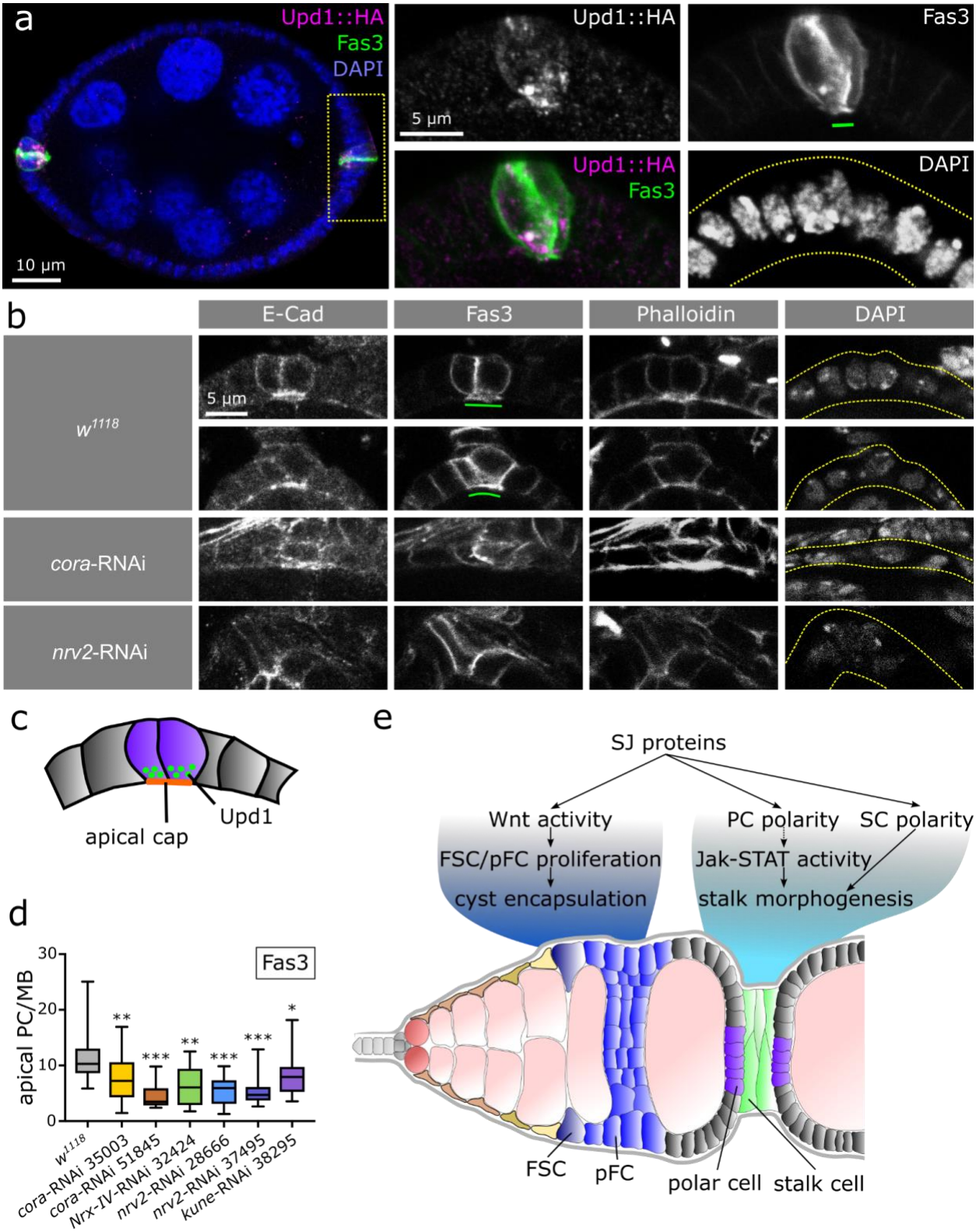
a
Upd1::HA
Fas3
DAPI
10 µm
Upd1::HA
5 µm
Fas3
Upd1::HA
Fas3
DAPI
b
E-Cad
Fas3
Phalloidin
DAPI
w1118
5 µm
cora-RNAi
nrv2-RNAi
c
apical cap
Upd1
d
Fas3
apical PC/MB
30
20
10
0
**
***
**
***
***
*
w1118
cora-RNAi 35003
cora-RNAi 51845
Nrx-IV-RNAi 32424
nrv2-RNAi 28666
nrv2-RNAi 37495
kune-RNAi 38295
e
SJ proteins
Wnt activity
PC polarity
SC polarity
FSC/pFC proliferation
Jak-STAT activity
cyst encapsulation
stalk morphogenesis
FSC
pFC
polar cell
stalk cell

Figure 6

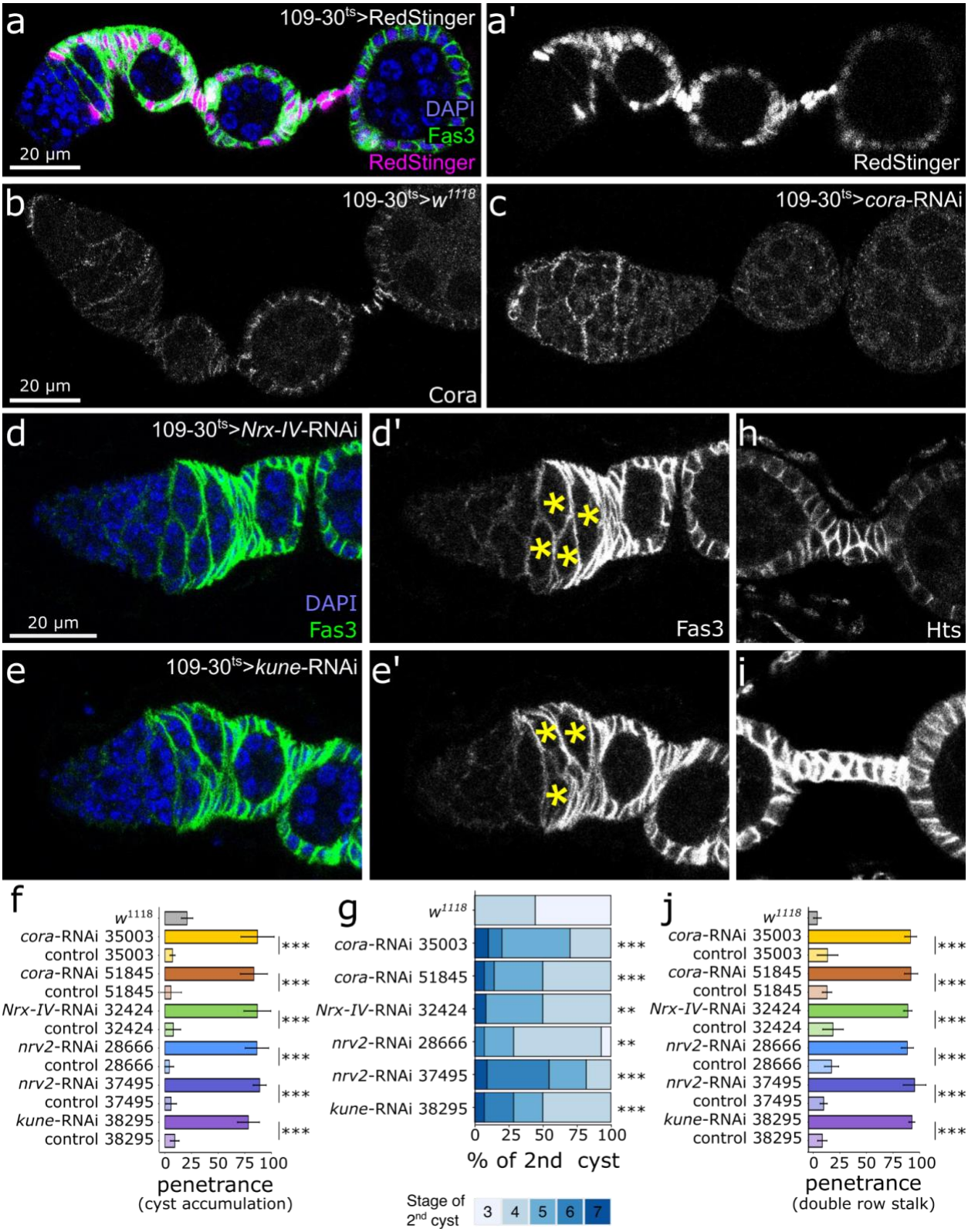
a
109-30ts>RedStinger
DAPI
Fas3
RedStinger
20 µm
a'
RedStinger
b
109-30ts>w1118
20 µm
Cora
c
109-30ts>cora-RNAi
d
109-30ts>Nrx-IV-RNAi
DAPI
Fas3
20 µm
d'
Fas3
h
Hts
e
109-30ts>kune-RNAi
e'
i
f
w1118
cora-RNAi 35003
control 35003
cora-RNAi 51845
control 51845
Nrx-IV-RNAi 32424
control 32424
nrv2-RNAi 28666
control 28666
nrv2-RNAi 37495
control 37495
kune-RNAi 38295
control 38295
***
0 25 50 75 100
penetrance
(cyst accumulation)
g
w1118
cora-RNAi 35003
cora-RNAi 51845
Nrx-IV-RNAi 32424
nrv2-RNAi 28666
nrv2-RNAi 37495
kune-RNAi 38295
***
**
0 25 50 75 100
% of 2nd cyst
Stage of 2nd cyst
3 4 5 6 7
j
w1118
cora-RNAi 35003
control 35003
cora-RNAi 51845
control 51845
Nrx-IV-RNAi 32424
control 32424
nrv2-RNAi 28666
control 28666
nrv2-RNAi 37495
control 37495
kune-RNAi 38295
control 38295
***
0 25 50 75 100
penetrance
(double row stalk)

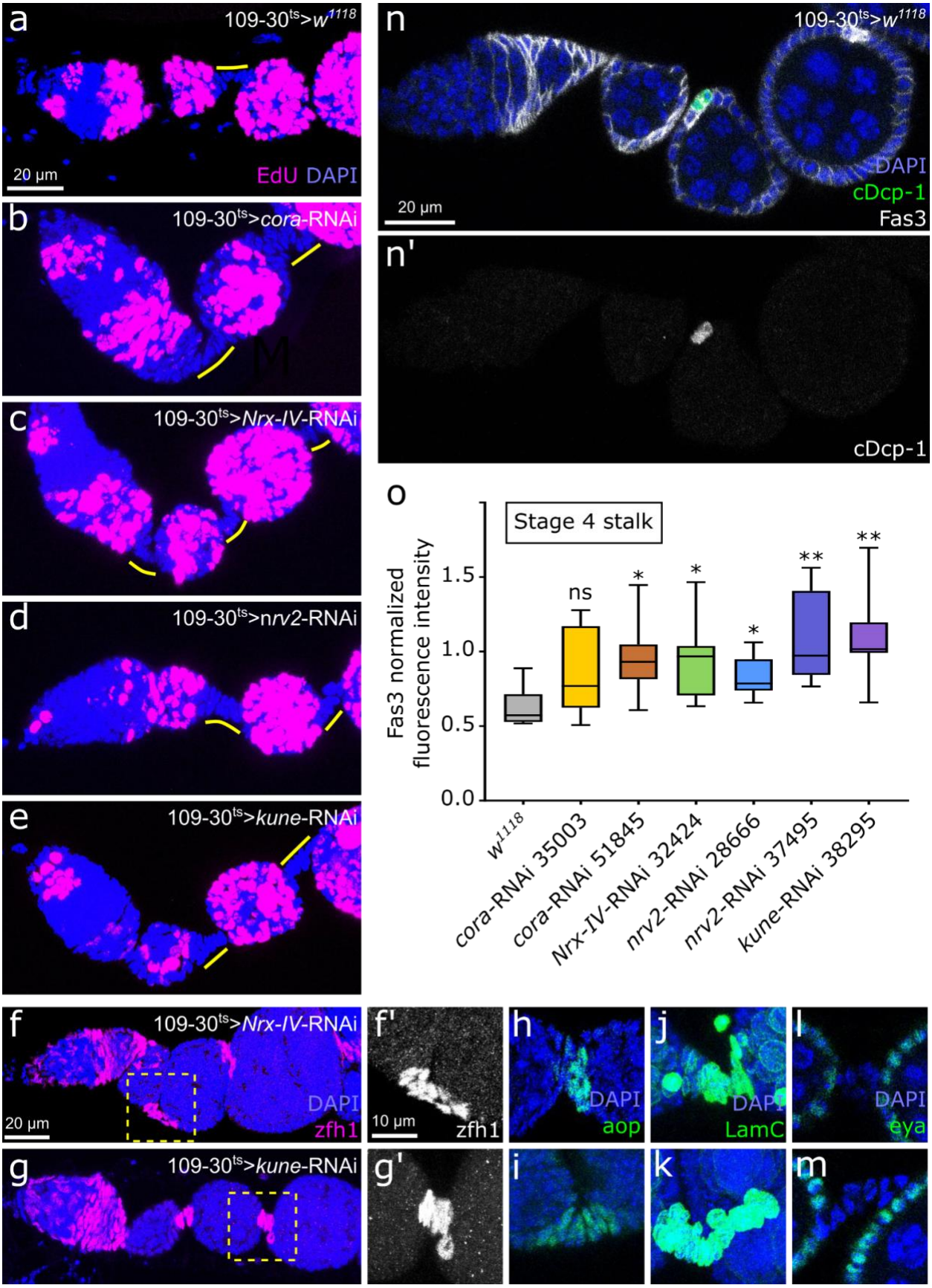
a
109-30ts>w1118
20 µm
EdU DAPI
b
109-30ts>cora-RNAi
M
c
109-30ts>Nrx-IV-RNAi
d
109-30ts>nrv2-RNAi
e
109-30ts>kune-RNAi
n
109-30ts>w1118
20 µm
DAPI
cDcp-1
Fas3
n'
cDcp-1
o
Stage 4 stalk
Fas3 normalized fluorescence intensity
0.0
0.5
1.0
1.5
ns
*
*
*
**
**
w1118
cora-RNAi 35003
cora-RNAi 51845
Nrx-IV-RNAi 32424
nrv2-RNAi 28666
nrv2-RNAi 37495
kune-RNAi 38295
f
109-30ts>Nrx-IV-RNAi
20 µm
DAPI
zfh1
f'
10 µm
zfh1
h
DAPI
aop
j
DAPI
LamC
l
DAPI
eya
g
109-30ts>kune-RNAi
g'
i
k
m

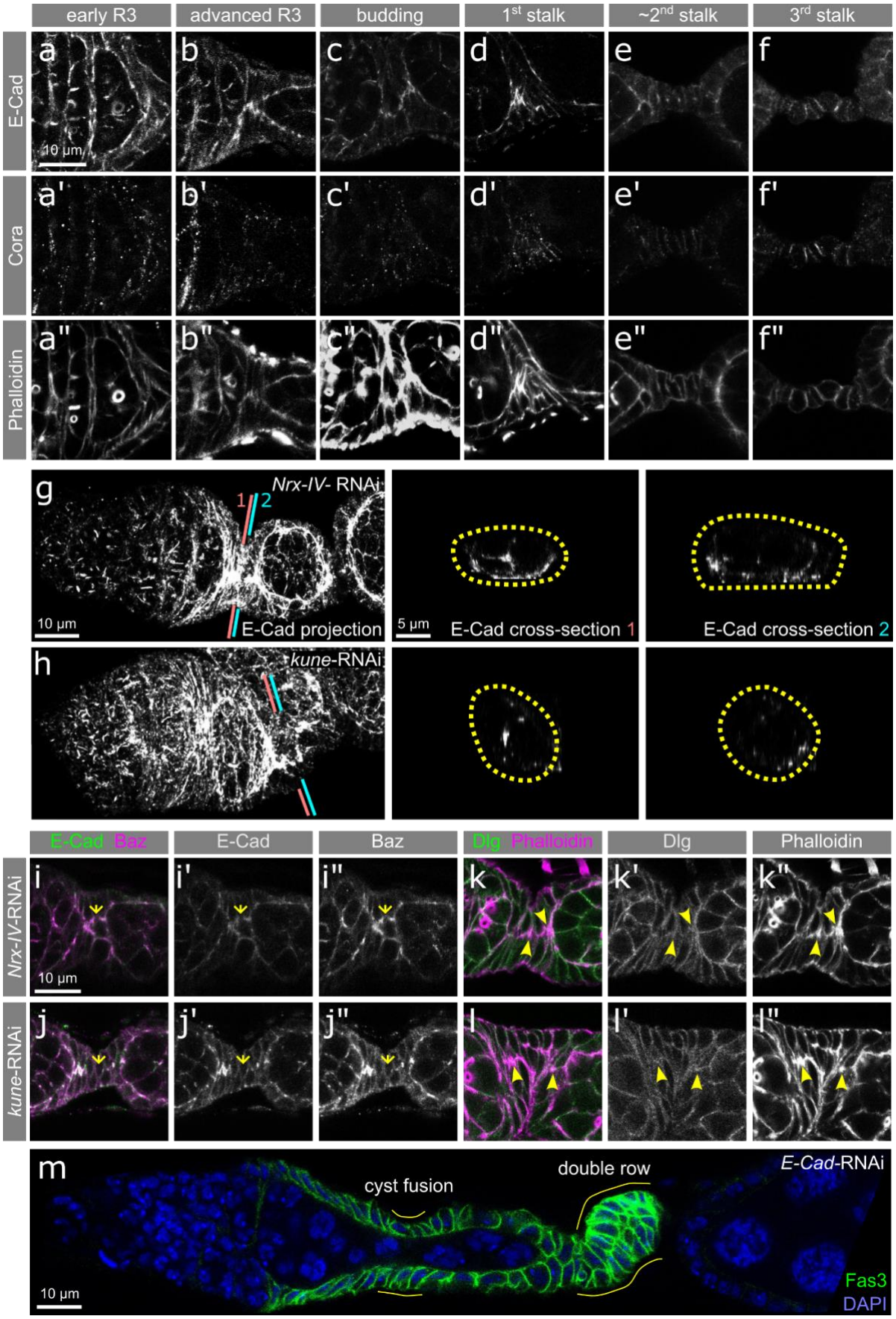

Supplementary Figure 3

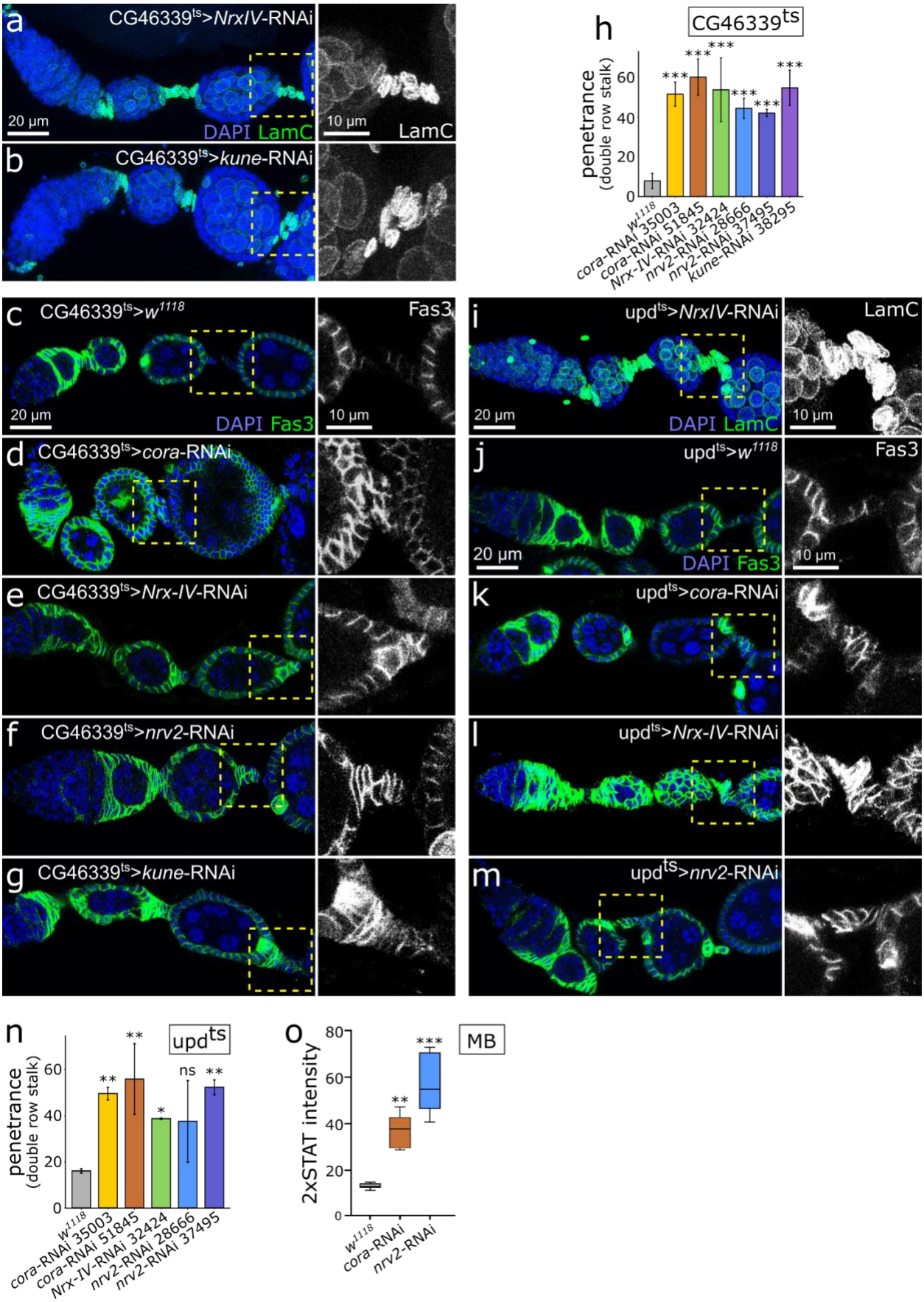

Supplementary Figure 4

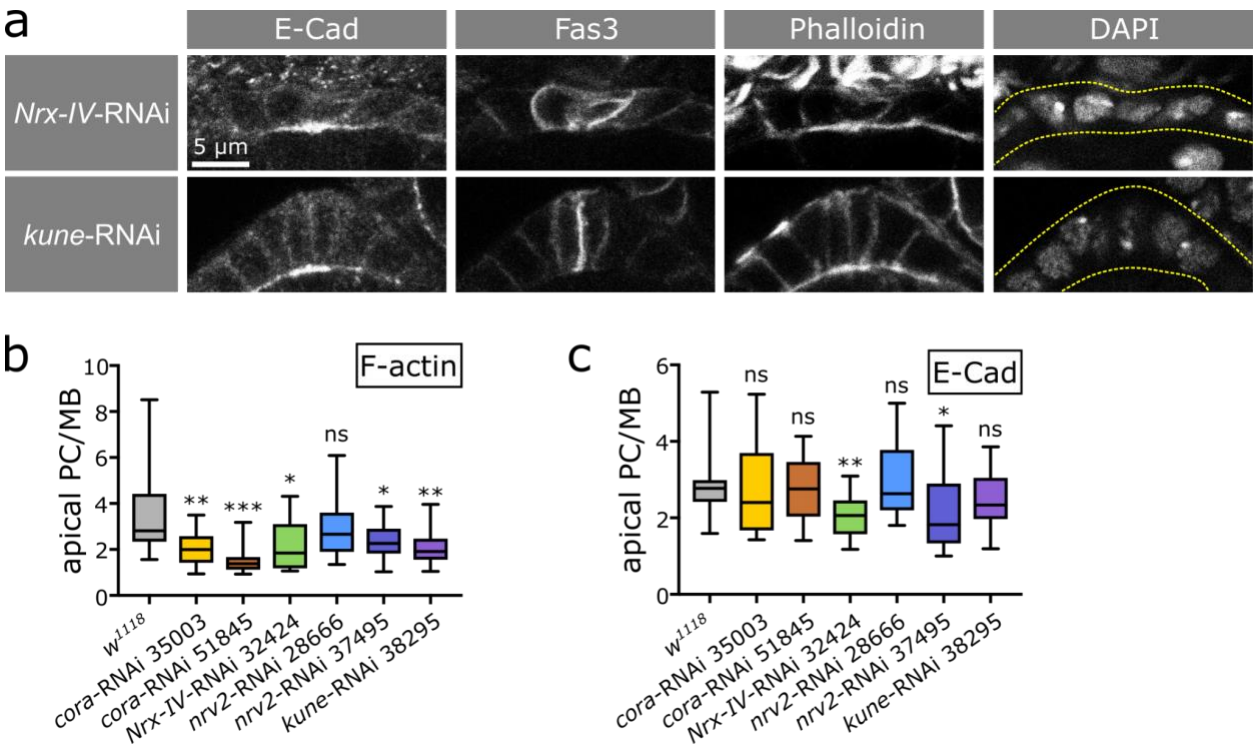
a
E-Cad
Fas3
Phalloidin
DAPI
Nrx-IV-RNAi
5 µm
kune-RNAi
b
F-actin
apical PC/MB
10
8
6
4
2
0
**
***
*
ns
*
**
w1118
cora-RNAi 35003
cora-RNAi 51845
Nrx-IV-RNAi 32424
nrv2-RNAi 28666
nrv2-RNAi 37495
kune-RNAi 38295
c
E-Cad
apical PC/MB
6
4
2
0
ns
ns
**
ns
*
ns
w1118
cora-RNAi 35003
cora-RNAi 51845
Nrx-IV-RNAi 32424
nrv2-RNAi 28666
nrv2-RNAi 37495
kune-RNAi 38295